Integrated generator for use in aircraft engines

Pre-study

Fredrik Andersson

LUNDS UNIVERSITET

Fakultet | Avdelning | Lunds universitet

ISRN LUTMDN/TMHP-18/5408-SE
ISSN 0282-1990

Tryckt i Sverige av Media-Tryck, Lunds universitet
Lund 2018

Table of Contents

Abstract

In this paper the use of integrated generators for airplane engines is examined. In order to accomplish this goal a combination of MatLab with FEMM and ANSYS Maxwell is used to make incrementally more and more detailed analysis of the integrated generator concept. After numerous numerical experiments and simulations it is concluded that the implementation of an integrated generator on the proposed RM400 engines should be possible, as well as contributing to overall improved fuel economy for the aircraft. However further analysis of the following is needed before further steps can be taken in the implementation of this concept:

- Optimization of design (power and weight)
- Structural solidity
- Heat transfer and cooling
- Power electronics
- Maintenance
- Safety
- Economics and manufacturing logistics

Acknowledgement

I would like to thank Dr. Avo Reinap at LTH for all the help he has provided during this project, as well as for his never failing patience.

I would like to thank Professor Magnus Genrup at LTH for putting this project together as well as for all he did in it.

I would like to thank both Engineering Method Specialist Richard Avellan and Company Specialist Hans Mårtensson at GKN for letting me do this project for you as well as for all the help and feedback you have provided me with during the course of this project.

Nomenclature

AC	Alternating Current
APB	Auxiliary Power Breaker
APU	Auxiliary Power Unit
ATRU	Auto-Transformer Rectifier Unit
BTB	Bus Tie Breaker
CSD	Constant Speed Drive
DC	Direct Current
EIS	Entry Into Service
EM	Electrical Machine
EPB	External Power Breaker
EPGS	Electrical Power-Generations Systems
EPS	Electric Power Systems
FEMM	Finite Element Method Magnetics
GCB	Generator Control Breaker
GCU	Generator Control Unit
IDG	Integrated Drive Generator
IFE	In-Flight Entertainment
IM	Induction Machine
JSF	Joint Strike Fighter
KC	Key Characteristics
MEA	More Electrical Aircraft
MTO	Max Take-Off
PAX	Passengers
PMM	Permanent Magnet Motors
PMMTLM	Permanent Magnet Motors Toothless Multipole
PMMTLTP	Permanent Magnet Motors Toothless Two-Pole
PMMTM	Permanent Magnet Motors Tooth Multipole
PMMTTP	Permanent Magnet Motors Tooth Two-Pole
PPD	Primary Power Distribution
PPP	Primary Power Panel
RMS	Root Mean Square
SFC	Specific Fuel Consumption
SPD	Secondary Power Distribution
SRM	Switched Reluctance Machine
TOC	Top of Climb
TRU	Transformer Rectifier Unit

1 Introduction

As aircrafts are getting ever bigger so is the onboard power need, this as a result of the increasing need for power in the flight system, transitions from typical pneumatic and hydraulic systems to modern electrical systems, as well as IFE. The power need per passenger can be approximated to 500W in “kitchen” power and 100W for IFE [1]. This gives that an Airbus A380 with a maximum passenger capacity of 525 people has a power need of 315kW just for the passengers.

When it comes to trends for EPS the most recent development is the variable frequency, both the Boeing 787 and the Airbus 380 utilizes this technology. Both these systems utilizes 400VAC at the primary bus (sum of 3-phases) and ATRU to convert the electricity to 270VDC in order to control actuation motors, hydraulic pumps and other large motors [2].

Another set of possibilities investigated by Boeing are to replace the current hydraulic networks and instead go over to using electrical actuators. There is also interest in using a “more electric engine” or an “all-electric engine” as well as looking in to using fuel cells for future aircraft travels [3].

One of the more direct implementations of having a large electrical generation from the engines is that instead of using bleed air from the motors to power the air-conditioning, this can be done with dedicated compressors powered by an EM. Such is the design on the Boing 787, this in turn gives a higher engine efficiency since less valuable bleed air is needed [4].

In order to get a better grasp of what can be considered good when it comes to electrical generation for aircrafts. The following compilation of modern aircrafts has been made (see table 1.1) [5].

Table 1.1.
Electrical power output for state-of-the-art aircrafts on the current market.

Aircraft	Electric power, kW	EIS	PAX	Power/PAX	MTOW, kg	Power/ MTOW	Engine
B787-8	1000	2011	242	4.132	227930	4.387	Trent 1000/GEnx
A380	600	2007	544	1.103	575000	1.043	GP7000/Trent 900
B737NG	180	1998	160	1.125	79010	2.278	CFM56
B717	80	1998	106	0.755	49900	1.603	BR715
A340	360	1993	335	1.075	276500	1.302	CFM56/Trent 500
B767	240	1982	243	0.988	204120	1.176	CF6-80/RB211-524/PW4056
B777	240	1995	313	0.767	247200	0.971	GE90
A350-900	400	2015	325	1.231	2.80E+05	1.429	Trent XWB

1.1 Aim

The goal of this project is to study the theoretical outcome of implementing a generator on the LP-shaft of a RM400 engine, with the aim of producing electrical power. The RM400 is a conceptual fan jet engine under development by GKN and has a rated thrust force of 84000 lbf (373650 N). The engine is developed for a "*widebody-aircraft*" similar to the Airbus A350 and has a planned life expectancy of 25 years. A few different generator configurations (A, B and C) have in advance been produced by GKN for evaluations. Expectations of what can be produced from the different configurations varies from 84 to 220 kVA of electric power at a voltage of 400/230VAC, for a rotational speed of 7362 rpm. The maximum outer dimensions can be seen in table 1.2 below.

Table 1.2.
Expected outcome for the different generator configurations

Configuration	Outer radius [mm]	Inner radius [mm]	Axial length [mm]	Expected power [kVA]
A	225	100	150	84
B	405	215	95	155
C	355	95	135	220

Another benefit of implementing this type of generator would be to remove the IDG (se chapter 1.4 for explanation). A component that is mechanically complex and subjected to a lot of wear and tear and is quite expensive (50,000 – 100,000 USD per unit). This wear gives the IDG a relatively low reliability responsible for a lot of flight schedule disturbances in commercial air flight, not to mention a safety concern. It would therefore be of great interest to remove this component from the electrical system [22].

For a better understanding of the placement of the EM a conceptual sketch can be found below (figure 1.1). It should however be mentioned that the exact placement of the EM inside the compressor housing varies depending on the configuration. For more detailed images se chapter *2.3 conceptual design*.

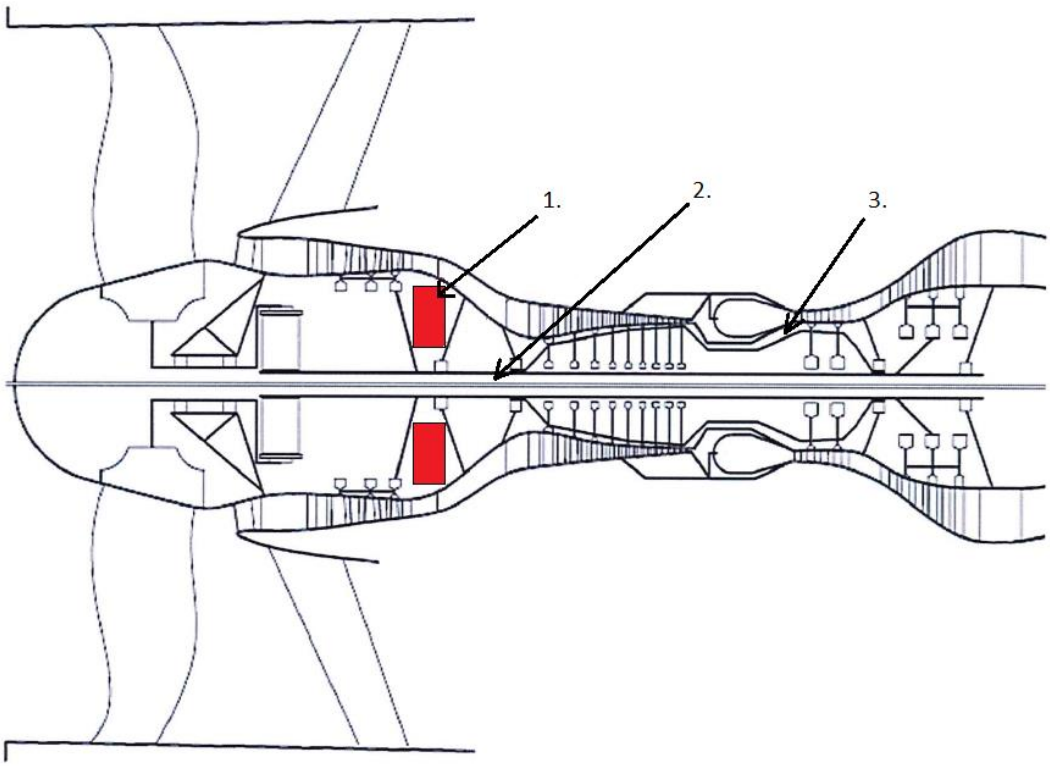

Figure 1.1.
Conceptual sketch of a turbofan engine where: 1 is the generator, 2 the Low Pressure Shaft (LPS) and 3 the High Pressure Shaft (HPS).

Listed in table 1.3 below are the operating conditions for the engine in question as well as minimum required electrical power output at these conditions. The parameter T24 represents the temperature surrounding the generator.

Table 1.3.
Rotational speed for the low pressure shaft as well as the temperature surrounding the generator ("PWX, hp" and "Power needed, kW" displays the same parameter just in different units).

	Ground idle	Cruise	MTO	TOC
LPS, rpm	1500 – 2200	6744	7362	7454
T24, K	300	400	475	424
Power need, kW	123	123	156,6	123

1.2 Limitations

There are some limitations to what exactly will be analyzed in this project and presented in this repport. Initially the idea was to make a complete heat transfer analysis of the generator. Unfortunately due to numerous complications, among other things problems with the software, this could not be done. There will not be any analysis of the solidity of the structure either, these limitations are a result of work load and lack of knowledge within the area. Furthermore in this paper only aspect concerning the engine itself will be evaluated. Data regarding how this type of generator affects the rest of the airplane electric system will therefore not be found in this paper.

1.3 Background

In the beginning of the 1990s the US Air Force together with the US Department of Defense founded the "more electric" initiative. This initiative had as a goal among other things to reduce the number of power transitions within the aircraft as well as to use more reliable and compact power electronics, electrical distribution system and starter/generators. This was done in an effort to decrease the cost of production as well as maintenance and upkeep of coming generations advanced weapon system [1].

A similar project is the MEA, where one off the goals is to construct a starter/generator directly on the power shaft of the airplane engine without any gear box. This would allow for less bleed air to be needed from the engines since all the internal system such as flaps, anti-ice, brakes, fuel pumps, air-conditioner and the main engine starter would be electrically powered [1].

Studies for civilian aircrafts predicts that implementing these changes could result in aircrafts becoming 2-5% cheaper to produce as well as decrease the fuel consumption with 2%. However there are other studies which have found that the production costs of new aircrafts would increase and that there therefore would be an optimum of exactly how much MEA implementations that should be done [1].

In a similar study regarding the implementation of an integrated generator on a F110-129 engine performed in 1995, they came to the conclusion that this kind of configuration should be possible without too many changes to the structure of the rest of the engine. It was also believed that this kind of EM could be used as a starter motor, however this is questionable since it is common practice to first start up the HP-shaft when starting a gas turbine [7].

1.4 Electric Power System

The EPS supplies the aircraft with its electric power. In figure 1.2 an image of a simplified electrical power system can be found. In reality the system is a bit more complicated as well as the fact that there is one of these system on either side of the aircraft [8].

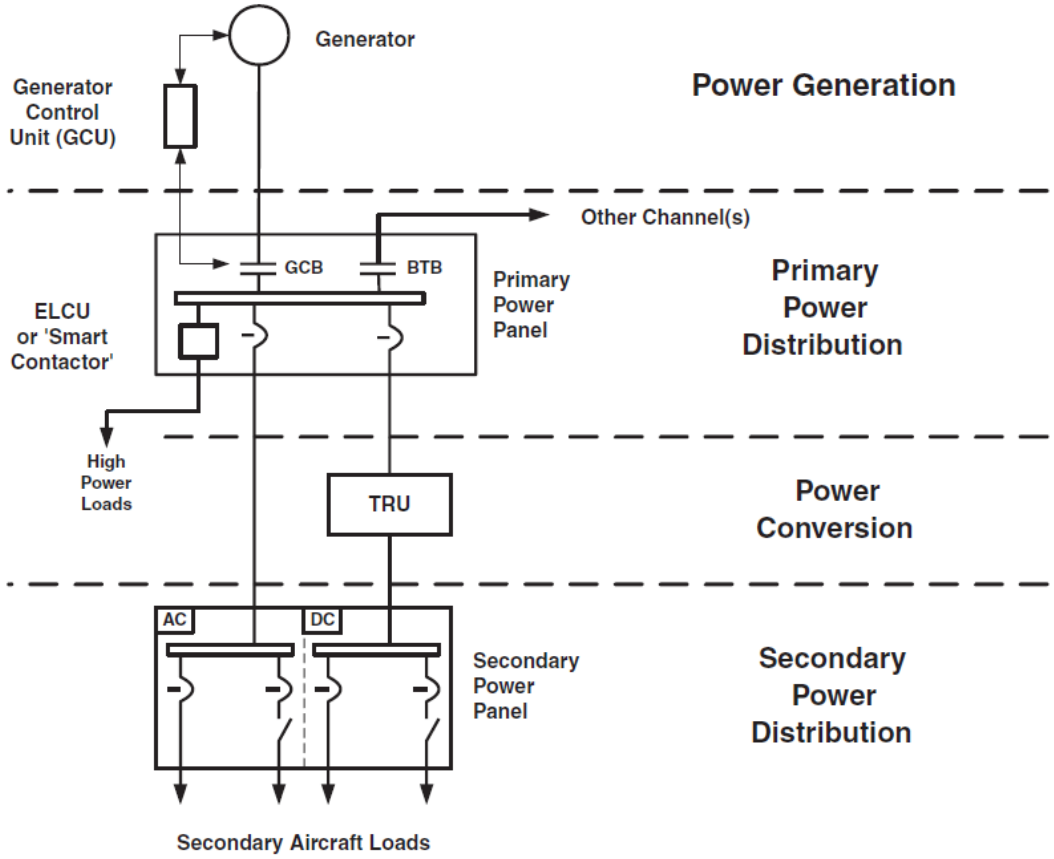

Figure 1.2.
Conceptual image of the power distrubution system, image original source [3].

1.4.1 Power Generation

Power generation is the part of the EPS in the aircraft where electrical power is generated. In a typical aircraft this is done by converting mechanical power through the accessory gearbox in to 115VAC, 3-phase, constant frequency 400Hz. The GCU then checks so that the power leaving the generator corresponds to these levels. Should this not be the case the GCU disconnects the generator from the PPD by opening the GCB [8].

Traditionally the electrical generation will be done with an IDG to provide the desired output. The IDG consists of two elements a CSD which maintains a constant rotational speed to the generator. This since the rotational speed on the main power shafts varies from 50 % when being idle on the ground to 100 % during active operations. The second part is the generator itself [8].

In more modern aircrafts, variable frequency generators have been used instead. These tends to be both cheaper and more reliable than traditional IDGs since the complex CSD element is removed. The variable frequency generator also generates less heat losses compared to its counterpart, but in return it also introduces some significant system issues for the high power inductive loads like the engines which have to be solved [8].

1.4.2 Primary Power Distribution

The PPD is where the main power distribution occurs, here there are a series of high power breakers like the GCB along others. These breakers also contain the BTBs that allows for the transferal of electrical power between the left and right EPS. Except for these there are also APBs that connects the PPD to the APU and finally the EPBs that allows the aircraft to be connected to an external AC power source [8].

Before reaching the PPP the electricity is feed along the main power feeders. There is however a few losses associated with this transferal of electricity, in order to keep the voltage drop low along the feeder a low resistance is essential. This in turn means a larger dimension on the power cables, resulting in a higher weight for the main power feeders. The amount of losses in the feeders is proportional to the square of the current flowing through the cables. There is therefore a tradeoff between a high voltage level which requires heavier cables but in turn have less losses and lower voltage lighter cables and more losses [8].

1.4.3 Power Conversion

In the Power Conversion section some of the aircrafts AC electrical power is converted to DC by the use of a TRU [8].

1.4.4 Secondary Power Distribution

The SPD serves to supply and protect the aircrafts secondary AC and DC loads. This is done using a number of switches and safeties [8].

1.5 Generator concept selection

When it comes to choosing what type of generator to use there are a lot of factors to consider such as: operation speed, cooling, power density and so on. In this paper the main focus will be placed on PMM specifically PMMTM, as it has been found to be the most promising candidate for this case [9].

While investigating the area it has been found that most studies indicate that PMM seems to be the most suitable solution for EPGS on board aircrafts.

PMM allows for both a high power density and high speeds. Another advantage is that most of the losses occurs in the stator, which is a desired feature for this project since it would be very complicated to cool the rotor. There are several different types of PMM to choose from as can be seen in figure 1.3, the yellow boxes shows EM used in EPGS today. Below figure 1.3

is table 1.4 which shows different EM suitability for the use in EPGSs based on 14 important KC which are discussed in more detail below [9].

The highest rated PMM and EM for that matter is the PMMTLM this will however not be the layout that will be investigated in this paper. Instead the focus will be on PMMTM, which has many advantages, high current density and power density are some of the most important. Compared to the PMMTTP the PMMTM is cheaper as well, this since it requires less back iron to close the magnetic circuit as well as less magnetic material for its PM. It can also be mentioned that both Lockheed's JSF and NASAs Next generation launch technology utilizes PMM for their EPGS. In figure 1.4 a cross section of this type of EM can be seen [9].

Another interesting option when it comes to the configuration of a generator is the choice between in-runner and out-runner. The difference between these two configurations is simply the placement, in most motors the rotor is placed inside the stator hence in-runner. For an out-runner the placement is simply changed so that the rotor is surrounding the stator (see fig 4.13). Equation (1.1) listed below (where P is electrical power generated, C is a machine constant, B_L is the magnetic load, AC is the specific electric loading, D is the rotor (at air-gap) diameter, L is the axial length of the machine and N is the shaft speed) gives an approximation of power output as a result of the listed input data. From this formula it is simple to deduct that an increase of speed on the rotor yields an increase in power density. It would therefore be of interest to look at the difference between an in-runner and out-runner configuration of the chosen PMM EM since they have different rotor velocity but otherwise mostly remain the same [9].

$$P = C \times B_L \times AC \times D^2 \times L \times N \qquad (1.1)$$

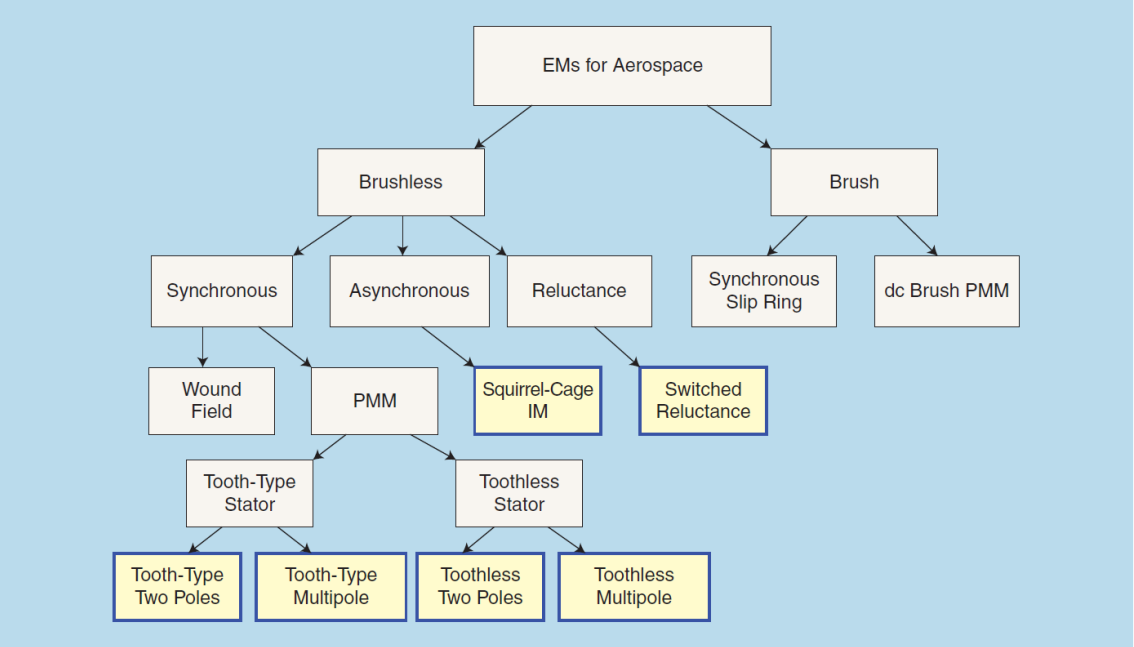

Figure 1.3.
Different types of EM as well as development path, image taken from [9].

Table 1.4.
Summation of suitability of EM for use as integrated generator, image taken from [9].

TABLE 1. Electric Machines Rated by Key Characteristics.

Machine-Type KCs*		Rating[1]					
		IM	SRM	PMM Tooth, Two-Pole	PMM Tooth, Multipole	PMM Toothless, Two-Pole	PMM Toothless, Multipole
KC 1	Rotor losses	6	6	10	10	10	10
KC 2	Stator losses	8	8	9	10	8	9
KC 3	Windage losses	5	1	9	9	10	10
KC 4	Rotor thermal limitations	8	10	4	4	4	4
KC 5	Cooling options	5	5	9	9	10	10
KC 6	Rotor mechanical limitations	5	7	9	9	10	10
KC 7	Torque-to-inertia ratio	5	7	9	9	10	10
KC 8	Torque pulsation	9	3	6	6	10	10
KC 9	Compatibility with bearings	5	5	9	9	10	10
KC 10	High-speed capability	5	7	9	9	10	10
KC 11	Short-circuit behavior	10	10	4	4	3	3
KC 12	Machine complexity	7	10	9	9	8	8
KC 13	Current density	7	7	10	10	8	8
KC 14	Power density	7	8	10	10	8	8
Total		92	92	116	117	119	120

*Descriptions of the KC numbers are provided in the section "Electric Machine Key Characteristics"
[1] 10=best, and 1=worst.

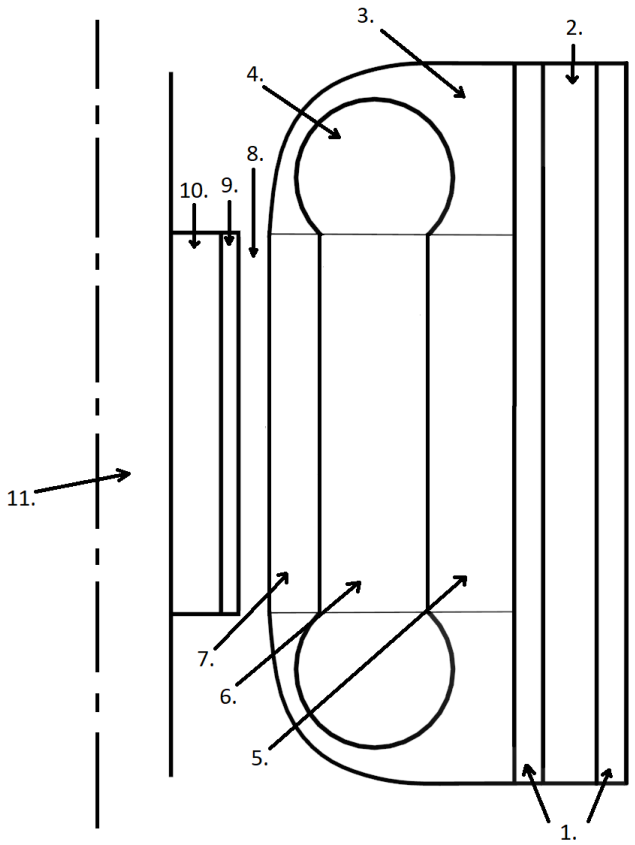

Figure 1.4.
Cross section of PMMTM in-runner with the following sections. 1=housing, 2=cooling channel, 3=cooling matrix, 4=windings, 5=iron core, 6=slot, 7=iron core/slot, 8=air gap, 9=magnets, 10=rotor and 11=low pressure shaft.

1.5.1 KC 1 Rotor losses

As the name applies rotor losses are the losses that occur in the rotor. High losses here can generate a lot of complex geometry within the generator since it can be very hard to cool the rotating part of a generator. Since all of the electrical generation occurs in the stator for the PMM EM and only minimal eddy current losses are present for the PMM very little heat is generated in the rotor. And by implementing composite sleeves even fewer losses can be achieved. This whilst both the IM and the SRM have much higher rotor losses [9].

1.5.2 KC 2 Stator losses

Also in this category the IM and SRM fares a bit worse than most of the PMM EM this due to better back iron utilization from the PMM EM. The reason for the somewhat higher losses from the toothless PMM compared to the tooth PMM is due to flux in the containment ring. But overall the machines have fairly similar stator efficiency due to fairly similar design [9].

1.5.3 KC 3 Windage losses

The windage losses are the losses that occur in the air gap between the rotor and stator. These losses are a function of the size of the gap, the rotor tip speed, the quality of the rotor and stators surfaces, the medium in the air gap as well as additional flow for cooling. PMM have a distinct advantage here because of their smooth surfaces as well as having a fairly large air gap, toothless have slightly less losses here due to their somewhat larger air gaps. Both the SRM and IM are rated lower the SRM for its complex rotor shape as well as the potential need to introducing additional gas flow for cooling. The IM scores low for its rough rotor surface as well as the need for additional gas cooling in the gap [9].

1.5.4 KC 4 Rotor thermal limitations

Rotor thermal limitation is a very important characteristic to take in to consideration since low values here can make the EM hard to use in a hot environment like an engine [9]. The PMM EM scores fairly low in this category since the PM are limited to around 260℃ (533 K), this is however based on the use of Samarium Cobalt magnets [10]. The SRM can be used in environments with a temperature of up to 400℃ with its steel lamination materials. The IM scores slightly lower since it utilizes copper or aluminum bars in its configuration. It should however not be forgotten that PMM have very small rotor losses which means that they generate very little heat on their own, so if the environment is not too hot they should work fine [9].

1.5.5 KC 5 Cooling options

When it comes to cooling, the PMM are rated high both due to the fact that they have minimal losses in the rotor, meaning that it does not need much cooling and in some cases due to the fact that the windings are exposed making it easy too cool. The same cannot be said about the IM and SRM which both scores much lower than the PMM EM [9].

1.5.6 KC 6 Rotor Mechanical Limitations

Rotor mechanical limitations are directly linked to the EMs ability to function at high speeds the, stiffness of the rotor is therefore of high importance in this characteristic. The PMMTL EM fares slightly better than their toothed counter parts, this is due to their low dependence on the air gap. After the PMM EM comes the SRM with its simple rotor design followed by the IM which embedded heavy bus bars makes it susceptible to large centrifugal forces at high speeds [9].

1.5.7 KC 7 Torque-to-inertia ratio

A high toque-to-inertia ratio means the ability to accelerate and decelerate very fast, this is typically very important for EPGS with self-start capabilities. In this characteristic dynamic and steady-state operations are traded to acquire a balanced performance. In this category PMM EM are the best followed by SRM and lastly the IM [9].

1.5.8 KC 8 Torque pulsation

Torque pulsation is a very important characteristic to take in to consideration when considering systems that are very sensitive to vibrations. A system that is not mechanically well damped can get excited by torque pulsation resulting in destructive consequences. There are two main types of torque pulsation in an EPGS, these are: 1, current pulsation in the stator winding and 2, cogging torque. This is a large problem for the SRM which is easily susceptible to torque pulsation, the cogging torque is a problem for the PMMT due to the interaction between the toothed stator and the PM in the rotor giving it a fairly low rating. The PMMTL on the other hand do not have any cogging torque giving it very smooth operation at sinusoidal stator currents. Since the IM have no PM it does not suffer from cogging torque it is however also required to have a sinusoidal current during power extraction [9].

1.5.9 KC 9 Compatibility with bearings

The EMs ability to function properly with different types of bearings is very important for EPGS, especially with the next generation foil- and magnetic bearings. This means that rotor stiffness as well as a large air gap is an advantage in this category. It is therefore no surprise that the PMMTL EM fares the best followed by the PMMT EM. Both SRM and IM EM are very sensitive to air-gap size making it a larger challenge for these machines to function with these new types of bearings [9].

1.5.10 KC 10 High-speed capability

High speed capability is more or less a summation of rotor mechanical losses, rotor losses windage losses, rotor thermal limitations and machine complexity. The PMM scores high in this mainly due to their high rotor stiffness and low sensitivity to the air gap [9].

1.5.11 KC 11 Short-circuit behavior

The short-circuit behavior is a measurement of the EMs ability to disable excessive currents in case of a failure. Due to the nature of the PMM all these EM scores low, it is not possible to turn off the electrical generation while the low pressure shaft is still spinning. There are however some PMM EM that are rated high because of their ability to create a high-reactance which significantly reduces the problem. Both the SRM and IM are rated high in this category since neither of them uses PM enabling them to shut down the electrical power generation within the electrical time constant [9].

1.5.12 KC 12 Machine complexity

Machine complexity can be placed in direct correlation to reliability, therefore the SRM is the best EM in this category due to its simple rotor design. After the SRM are the PMM EM because of its simple and robust rotor construction, PMMTL fares slightly worse here due to the additional ring around the stator for stray flux containment. The IM however has a more complex design scoring it slightly lower than the others [9].

1.5.13 KC 13 Current Density

The current density is the EMs capacity to be loaded with certain ampere turns per unit surface of the outer diameter. This value is in direct proportion to the cooling integration and possibility of the EM, in this category the PMMT are the best. This is due to their low losses as well as the ability to cool the main stator ring directly, something that is not possible with the PMMTL EM. The IM and SRM have lower current density due to additional rotor losses as well as overall lower efficiency [9].

1.5.14 KC 14 Power Density

The power density category is a summation of several other characteristics and can be divided either by weight or volume. The highest ranking in this category is the PMMT EM due to many practical implementations followed by the PMMTL EM and at the bottom the SRM and IM [9].

2 Design models and modeling methods

2.1 Electric machine parts and geometric model

The purpose of this sub chapter is too look at what different models are used to analyze the problem at hand.

2.1.1 MatLab model

A first attempt of simulating the behavior of the generator is done using a custom made MatLab code written by Dr. Avo Reinap at LTH. This code utilizes the parameters listed in tables 2.1-2.4 and creates a 2D version of the EM that is to be investigated. This model gives operating temperatures and the magnetic flux inside the structure among other things. This is done using FEMM which is a separate toolset that can be used in connection with MatLab. With the help of this tool it will be possible both to run thermal analyses of the problem as well as electromagnetic. The results produced are however not deemed to be all too reliant. The MatLab code does nevertheless allow for fast set up of geometrical layout of the generator at hand which can then be used in later models. Most of the parameters used in the MatLab code are entered manually by the user, however a few of the inputs in the code are set so that they change dependent on other inputs, but this can of course be changed if one wishes it.

Table 2.1.
MatLab inputs listed under "*main machine design and modelling parameters*".

Input	Effect	Independent/dependent
Inner rotor motor enable	0 = out-runner configuration 1 = in-runner configuration	Independent
Number of poles	This input simply tells the code how many poles the EM will have.	Independent
Stator slot per phase and per pole	Winding configuration, needs to be divisible with the number of phases.	Dependent
Relative width of machine	Axial length of the machine in proportion to the outer diameter of the machine.	Independent
Relative inner radius for the machine	Inner radius of the machine in proportion to the outer radius.	Independent
Height of air-gap	Height of the air-gap that separates the stator from the	Independent

	rotor.	
Height of permanent magnets	Height of permanent magnets with base at the outer radius of the rotor.	Independent
Outer radius of machine	Outer radius of the EM.	Independent
Initial current density	Density of the current going through the electrical wiring.	Independent
Initial flux density	The initial maximum magnetic flux when the FEMM analysis starts.	Independent
Coil hot-spot temperature	Initial temperature at the hot-spot of the electrical wiring.	Independent
Ambient temperature	Temperature of the surrounding area.	Independent
Supply magnetization frequency	Frequency of the electrical current leaving the generator.	Independent
Convection factor	The heats ability to pass to the surrounding air.	Independent
In tube convection factor	Convection factor to the shaft.	Independent
In tube convection temperature	Ambient temperature of the shaft.	Independent
Slotting factor	Relative slot with where 0.1 is small and 0.9 is large.	Independent
Gap radius factor	Relative height of the gap where 0.1 is short and 0.9 is tall.	Independent

There are also some inputs for “Parameters” for the EM found in table 2.2. Most of these are controlled by the initial input found in table 2.1, however some are changed independently.

Table 2.2.
MatLab inputs listed under "*parameters*".

Input	Effect	Controlled/Independent
Number of poles	Number of poles	Controlled
Stator sloth per phase and per pole	Winding configuration, needs to be divisible with the number of phases.	Controlled
Winding fill factor	How much of the tooth gap that is filled with winding	Independent
Relative total angular with of the magnet	The area of the magnet with in proportion to the pole size.	Independent

Slotting factor	Relative slot with where 0.1 is small and 0.9 is large.	Controlled
Slot opening factor	Relative size of the opening for the gap where 0.1 is small and 0.9 is large.	Independent
Outer radius of stator	Outer radius of stator.	Controlled
Gap radius	Radius for the center of the air gap.	Controlled
Inner radius	Inner radius of the machine.	Controlled
Thickness of permanent magnets	Height of permanent magnets with base at the outer radius of the rotor.	Controlled
Gap length	Height of the air-gap that separates the stator from the rotor	Controlled
Thickness of insulation	Thickness of insulation.	Independent
Active length	Axial length of machine.	Controlled
Frequency	Frequency of the electrical current leaving the generator.	Controlled
Initial current density	Density of the current going through the electrical wiring.	Controlled
Maximal flux density in the core	The initial maximum magnetic flux when the FEMM analysis starts.	Controlled
Coil hot-spot temperature	Initial temperature at the hot-spot of the electrical wiring.	Controlled
Ambient temperature	Temperature of the surrounding area.	Controlled
Convection factor	The heats ability to pass to the surrounding air.	Controlled
FE mesh density	Resolution of the FEMM plot.	Independent
Displacement radius and angle in order to select a region	Displacement radius and angle in order to select a region in the FEMM plot.	Independent

Finally there are a set of inputs for “machine geometry formulation” found in table 2.3. Just like for the “Parameter” input most of these are controlled by the initial inputs but some are independent.

Table 2.3.
MatLab inupts listed under "*machine geometry formulation*".

Input	Effect	Controlled/Independent
Number of slots	Number of slots in the stator.	Controlled
Number of discrete magnets per pole	Number of smaller magnets in each large magnet in the EM model.	Independent
Thickness of housing	Thickness of the housing surrounding the EM	Independent
Top radial height of the tooth-tip (slot opening side)	Top radial height of the tooth-tip (slot opening side).	Independent
Bottom radial height of the tooth-tip (tooth side)	Bottom radial height of the tooth-tip (tooth side).	Controlled
Inner radius of rotor core	Inner radius of the EM.	Controlled
Outer radius of machine	Outer radius of the EM.	Controlled
Tooth width	Width of the tooth in the stator.	Controlled
Thickness of stator yoke	Thickness of stator yoke.	Controlled
Tooth width	Width of tooth in stator.	Controlled
Thickness of stator yoke	Thickness of stator yoke.	Controlled
The half of the outermost tooth angle.	The half of the outermost tooth angle.	Controlled
Yoke thickness for rotor	Yoke thickness for rotor.	Controlled
The half of sloth + tooth angle	The half of sloth + tooth angle.	Controlled
The half of innermost tooth angle	The half of innermost tooth angle.	Controlled
The half of tooth tip angle	The half of tooth tip angle.	Controlled
Total angular with of permanent magnet	Total angular with of permanent magnet.	Controlled
Offset angle for the magnet	Offset angle for the magnet.	Controlled

Together all of these values generate a geometrical layout as well as a visualization of magnetic flux and heat distribution within the EM, in accordance to what can be seen in figure 2.1 below. It should be mentioned that the images displayed has no integrated cooling in the housing, this will not be the cases for the simulations run in later chapters. The reason for this were problems with getting MatLab to draw the cooling channels in a proper way.

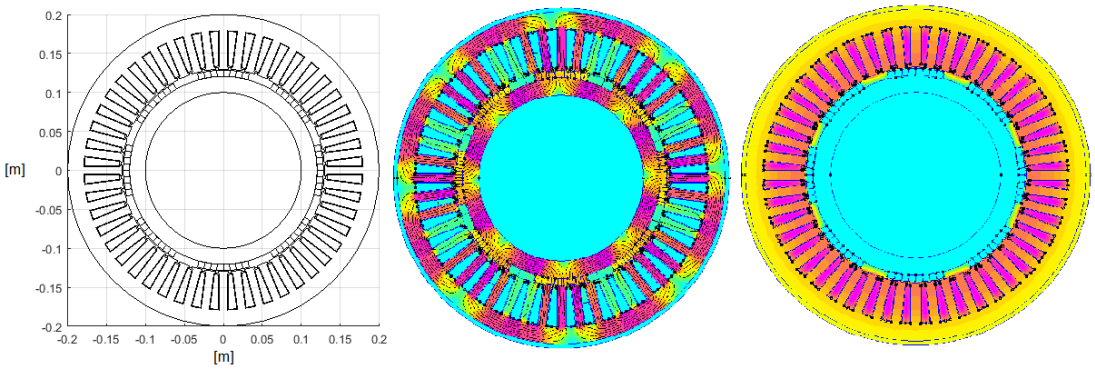

Figure 2.1.
Image of the EM as displayed in MatLab. To the left dimensions, in the middle the magnetic flux [T] and to the right the temperature [K] distribution.

During the initial stage of the use of the MatLab code a few extra parameters were added to control cooling, these parameters can be seen in the table below. It should also be mentioned that the parameter “thickness for cooling belt” takes the place of “thickness of housing” and the “thickness of housing” parameter is therefore dependent on this value instead of being independent as it initially was.

Table 2.4.
Additional MatLab inputs for cooling listed under "*main machine design and modelling parameters*".

Input	Effect	Controlled/Independent
number of cooling channels	Selects the number of cooling channels in the structure	Independent
thickness for cooling belt	Gives the thickness of the outer housing of the EM which contains the cooling channels	Independent
coolant temperature	Temperature of the coolant in the cooling system.	Independent

2.1.2 Maxwell RMxprt Design

Maxwell RMxprt Design is similar to the MatLab code, this program also performs a 2D analysis of the problem. RMxprt does not however display the magnetic flux or heat distribution like the MatLab code does. The amount of controllability of Maxwell RMxprt Design is nevertheless higher by default, allowing for more controllability for the user. In this program more accurate outputs for the generator can be calculated in all from electrical output to current density. This program does not utilize the finite element method however instead utilizing estimative formulas.

2.1.3 Maxwell 2D

Maxwell 2D offers a more advanced 2D analysis than RMxprt. Whilst the RMxprt based its analysis on estimative formulas the Maxwell 2D toll utilizes the finite element method to analyze the problem. From this model numerous properties can be calculated such as: torque, losses and induced voltage, to mention a few.

2.1.4 Maxwell 3D

Maxwell 3D is a far more advanced tool than the RMxprt previously used, it is however also much slower. This software allows for a much more detailed an in depth analysis of the machine for one set of operating conditions at the time. The software gives a more detailed image of the behavior of the machine as a function of time as well as a more realistic image of the losses for the EM. This model utilizes the same type of inputs as the 2D model.

Another important thing that can be done with Maxwell 3D is to estimate the width of the windings sticking out on the sides of the generator. This is also a very important aspect to take in to consideration since the space available for the generator is limited.

2.2 Coupled problem, coupled model

Many of the parameters for the machine control several aspects of its behavior. In this sub chapter two important parameters will be discussed as well as the resulting generator behavior from them.

2.2.1 Current for torque and current for heat

The amount of current flowing through the generator controls both the torque produced by the generator as well as the heat. The reason for this can be seen in equation (2.1) and (2.2) below.

$$\tau = k_t \cdot I \qquad (2.1)$$

Where τ is torque, k_t a constant and I current.

$$P_{Lw} = I^2 \cdot \frac{\rho l}{A} \qquad (2.2)$$

Where P_{Lw} are losses in winding, I current, ρ material resistivity, l length of winding and A the cross-section area.

As can be seen in equation (2.1) the torque is proportional to the current flowing through the generator assuming that the other parameters stays the same. The same thing is true for the losses due to current as can be seen in equation (2.2). Up to a certain point the torque gained however outweighs the losses. This can be seen in figure 2.2 below where the efficiency is plotted as a function of current for configuration *A 10p 60sl (5) out-runner* at a constant speed of 6744 rpm [11].

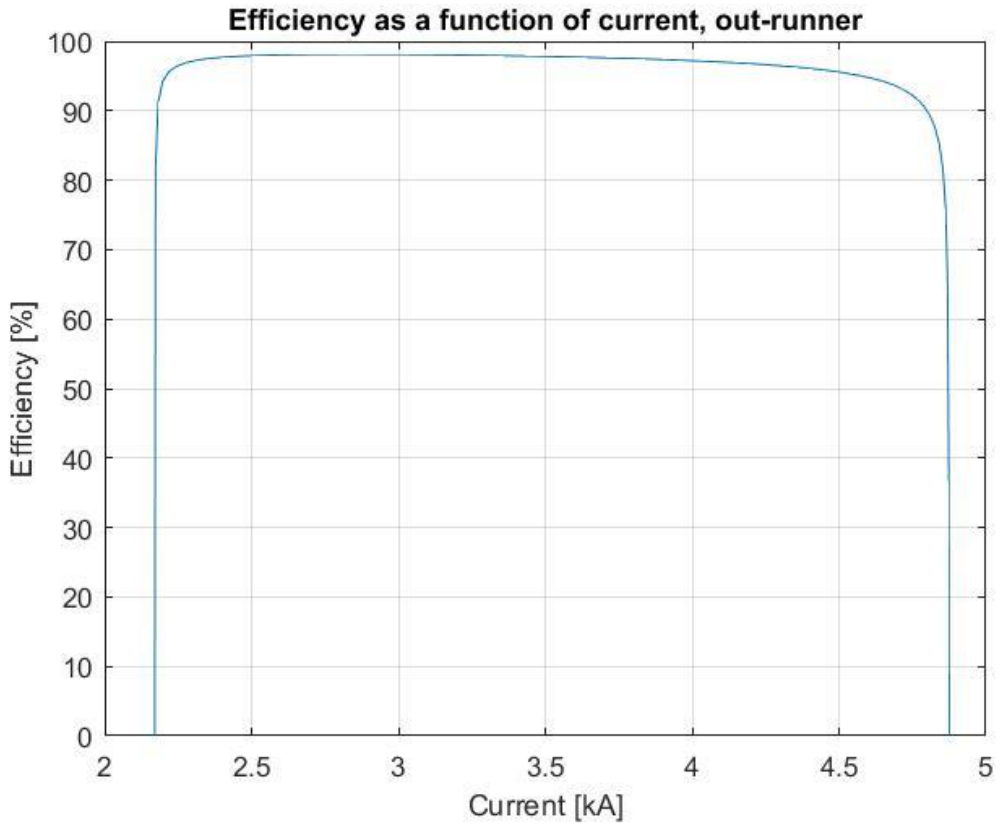

Figure 2.2.
Efficiency as a function of current at an operational speed of 6744 rpm.

2.2.2 Speed for power and speed for selfloading by losses

The speed of the rotor is another very important parameter for the behavior of the generator. A higher speed allows for more electricity to be produced as well as increase the amount of losses due to eddy currents. The reason for this can be seen in equation (2.3) and (2.4) below.

$$P = rpm \cdot \frac{\tau}{9.55} \qquad (2.3)$$

Where P is power, rpm revolutions per minute and τ torque [12].

$$P_{Lf} = f(rpm) \qquad (2.4)$$

Where P_{Lf} are losses due to frequency, f an arbitrary function and rpm revolutions per minute [13].

As can be seen in equation (2.3) the power is proportional to the speed of the rotor assuming that the other parameters stays the same. The same thing is true for the losses due to eddy currents for the generator as can be seen in equation (2.4). Overall the power gained however outweighs the increased losses from increasing the speed of the rotor (up to maximum power). This can be seen in figure 2.3 below where the efficiency is plotted as a function of power for configuration *A 10p 60sl (5) out-runner* at a speed between 1500 and 7454 rpm.

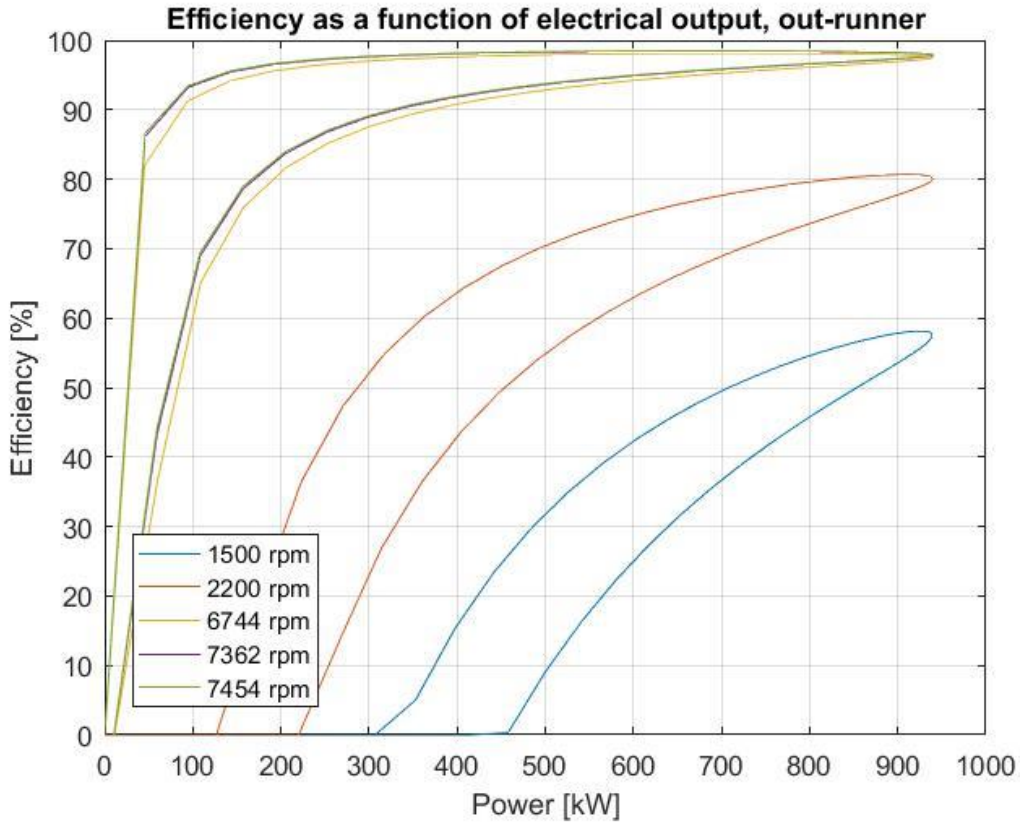

Figure 2.3.
Efficiency as a function of electrical power at different operational speeds.

2.3 Derivation of design parameters and space

Originally there where three different placements for the generator within the compressor housing. Each of these three spaces had their own advantages and disadvantages compared to one and other. Eventually configuration A was found to be the most prominent candidate for the generator, more in depth discussion of why can be found in this subchapter.

2.3.1 Configuration A

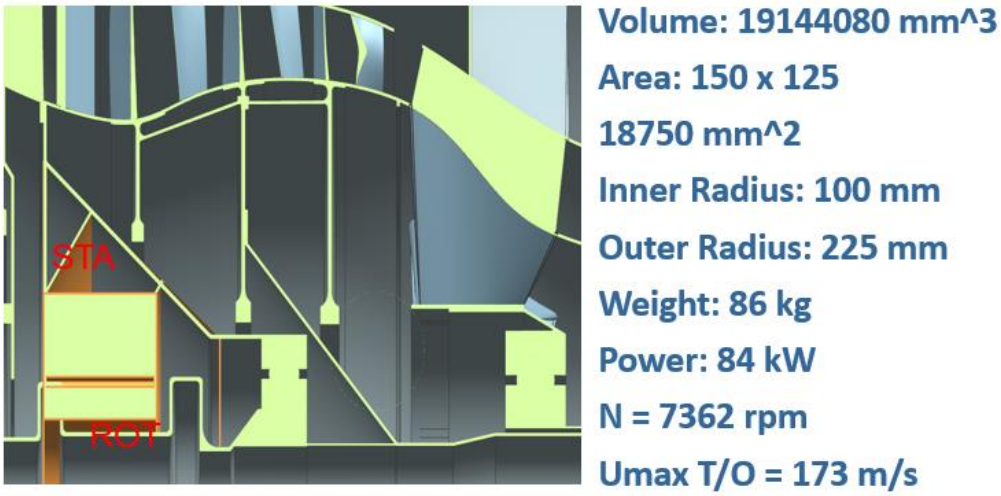

Figure 2.4.
Conceptual layout for configuration A with dimensions and estimated values for weight and power output.

In order to get a first preliminary grasp of how large of an electrical output the EM would have at the different spaces the following simple approximations seen below was used. When approximating torque of an in-runner EM it can be assumed that the torque is proportional to the shear stress at the rotor surface according to the following equation:

$$T = 2\pi r^2 l\sigma \qquad (2.5)$$

The dimensions for configuration A are set to $l = 0.15\ m$ and $r = 0.15\ m$ this value is however based on a guess since the outer rotor diameter is not set just jet. In accordance with [10] the shear stress σ can be assumed to be between $20{,}7\ kN/m^2$ and $34{,}7\ kN/m^2$ [10]. In order to not overestimate the expected power of the generator the shear stress was set to $20{,}7\ kN/m^2$. The calculated torque could then be converted to power by the use of the following equation:

$$P = rpm \cdot T/9.55 \qquad (2.6)$$

When this is done the same problem could be run using the MatLab code. There are five different operating speeds that are of interest to look at when running this problem. These speeds can however be divided in to two groups themselves when it comes to the MatLab simulations and these are operations with thermal inertia and operations without thermal inertia. For the simulations with thermal inertia the shaft temperature is assumed to be 350K as the temperature is on its way up to the cruise temperature 400 K. The simulations belonging to this group are 1500, 2200, 7362 and 7454 rpm. The operation without thermal inertia is therefore only the 6744 rpm operation, during this operation the temperature is as mentioned set to 400 K. The highest allowed temperature for the coil of the generator is determined by the isolation class. The sturdiest isolation class has an allowed temperature of 180C (453K) it should however be mentioned that a lower temperature on the windings will greatly improve the life expectancy of the generator [14]. The magnets have as mentioned an allowed maximum temperature of 260C (533K). The “coil hot-spot temperature” can be assumed to be approximately 445K. Since the surrounding air has a temperature of up to 475K air cooling will not be an option. Instead it is assumed that the EM is oil cooled a temperature of 95C (368K).

To allow MatLab to run this kind of problem cooling channels have been added in to the structure. It is then a simple matter of balancing the heat from the EM and the cooling from the oil so that it does not overheat. The new inputs that controls the cooling channels can be found under chapter *2.1 MatLab model* and are listed in table 2.4. Using the new model with imbedded cooling channels the oil temperature is set to 95C (368 K). The number of cooling channels is set to 70 and the thickness of the cooling belt to 25 mm. The reason for having 70 cooling channels can be found in chapter *2.4 Cooling MatLab VS Maxwell*.

To generate electricity magnets are used to attract and repel electrons inside the wiring. The best way to keep the electrons moving would therefore be to repel in one end of the wire and attract in the other. This means that the number of stator slots should be three times two times the number of poles for the wiring layout chosen for this machine. So for a six pole machine the number of stator channels should be 36 and so on, for a better understanding of why this is se figure 2.5 below.

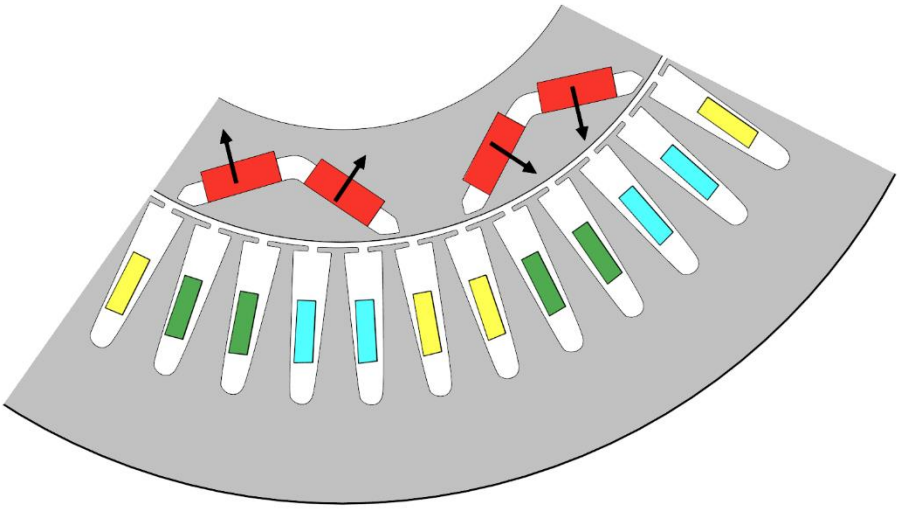

Figure 2.5.
Conceptual sketch of wire channel configuration and magnet placement inside the EM.

In the initial simulations with configuration A the input values listed in table 2.5 below where used.

Table 2.5.
Input values for simulations concerning configuration A.

Configuration	Outer radius of stator core	Relative inner radius for the machine	Relative width of machine	Slotting factor	Gap radius factor
6p 36sl test	200 mm	0.5	0.75	0.5	0.6
8p 48sl test	200 mm	0.5	0.75	0.5	0.6
10p 60sl test	200 mm	0.5	0.75	0.5	0.6
8p 48sl	200 mm	0.5	0.75	0.6	0.85
10p 60sl	200 mm	0.5	0.75	0.5	0.85

2.3.2 Configuration B

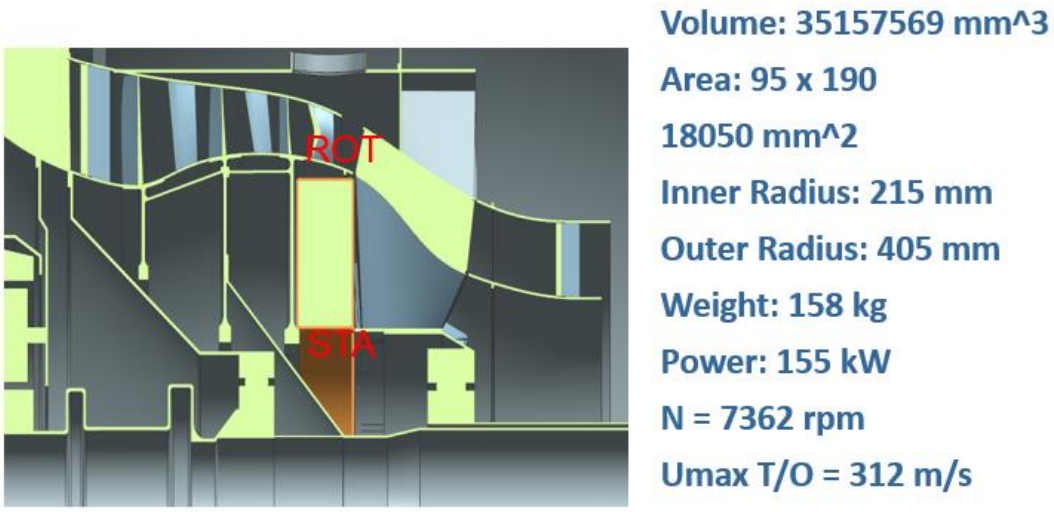

Figure 2.5.
Conceptual layout for configuration B with dimensions and estimated values for weight and power output.

Configuration B was then tested the same way as A. Initially by the use of equation (2.5) and (2.6) with $l = 0.095\ m$ and $r = 0.27\ m$.

However while running the selected dimensions in the MatLab code it was concluded that the machine was too thick, meaning that the coils where too far away from the cooling channels making it very hard to maintain acceptable temperatures on the coils, for a better understanding of the problem se figure 2.6 below. The machine was therefore re-sized so that this problem could be removed, both a six pole and an eight pole configuration was tested just as for Configuration A. The maximum allowed outer radius for the six pole machine was found to be 390 mm and for the eight pole version this dimension was 350 mm. By comparing the output from these machines it was found that the eight pole configuration was the better choice with a predicted torque of 812.8 Nm.

In the initial simulations with configuration B the input values listed in table 2.6 below where used.

Table 2.6.
Input values for simulations concerning configuration B.

Configuration	Outer radius of stator core	Relative inner radius for the machine	Relative width of machine	Slotting factor	Gap radius factor
10p 60sl (Overheated example)	380 mm	0.56579	0.25	0.45	0.6
8p 48sl	350 mm	0.61429	0.27143	0.4	0.7

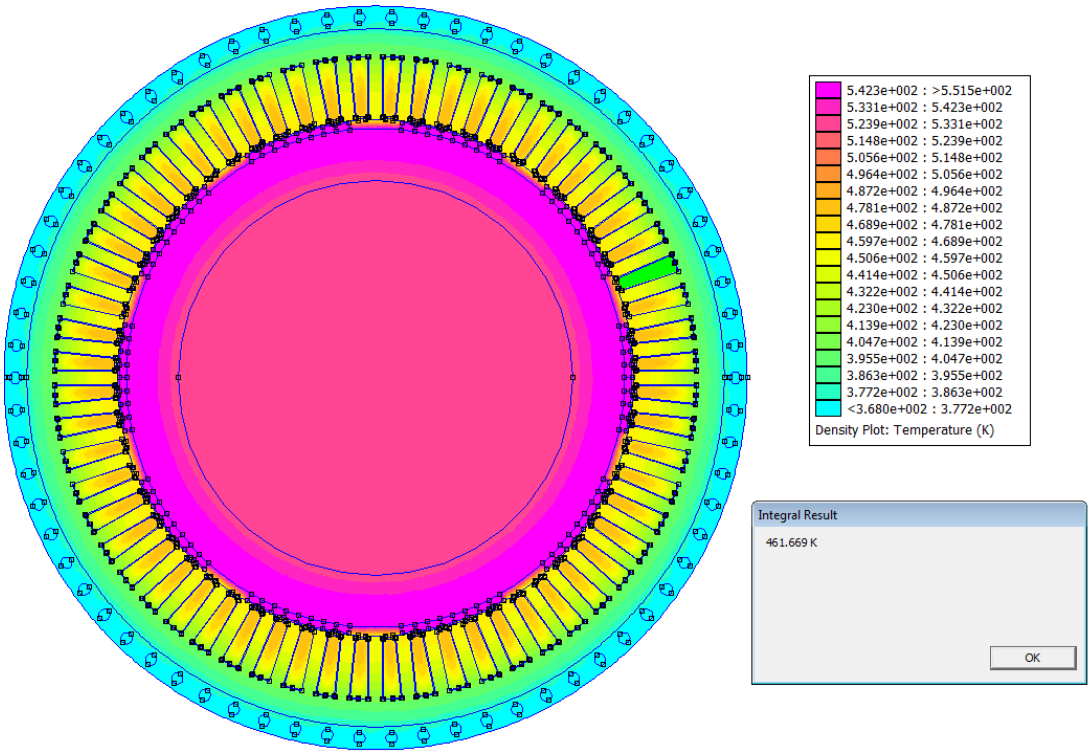

Figure 2.6.
Temperature distribution for the full scale configuration B, multiple test where run, none with acceptable winding temperatures.

2.3.3 Configuration C

Finally Configuration C was tested, initially using equation (2.5) and (2.6) with $l = 0.135\,m$ and $r = 0.15\,m$ and then MatLab. However when running the selected dimensions in the

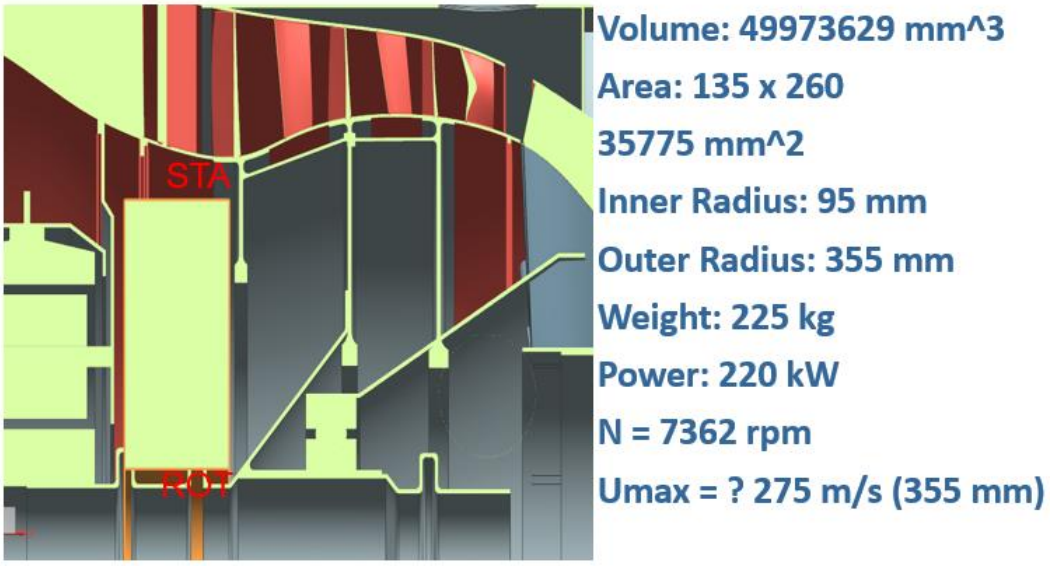

Figure 2.7.
Conceptual layout for configuration C with dimensions and estimated values for weight and power output.

MatLab code the same problem was encountered as when running configuration B, for a better understanding of the problem se figure 2.8 below. The machine was too wide to allow for an efficient cooling so resizing was made. It was found that a six pole configuration was possible using an outer radius of 270 mm. And for the eight pole configuration the maximum allowed outer radius was 250 mm.

In the initial simulations with configuration C the input values listed in table 2.7 below where used.

Table 2.7.
Input values for simulations concerning configuration C.

Configuration	Outer radius of stator core	Relative inner radius for the machine	Relative width of machine	Slotting factor	Gap radius factor
10p 60sl (Overheated example)	330 mm	0.28788	0.40909	0.5	0.6
8p 48sl	250 mm	0.38	0.54	0.35	0.7
6p 36sl	270 mm	0.34545	0.5	0.33	0.7

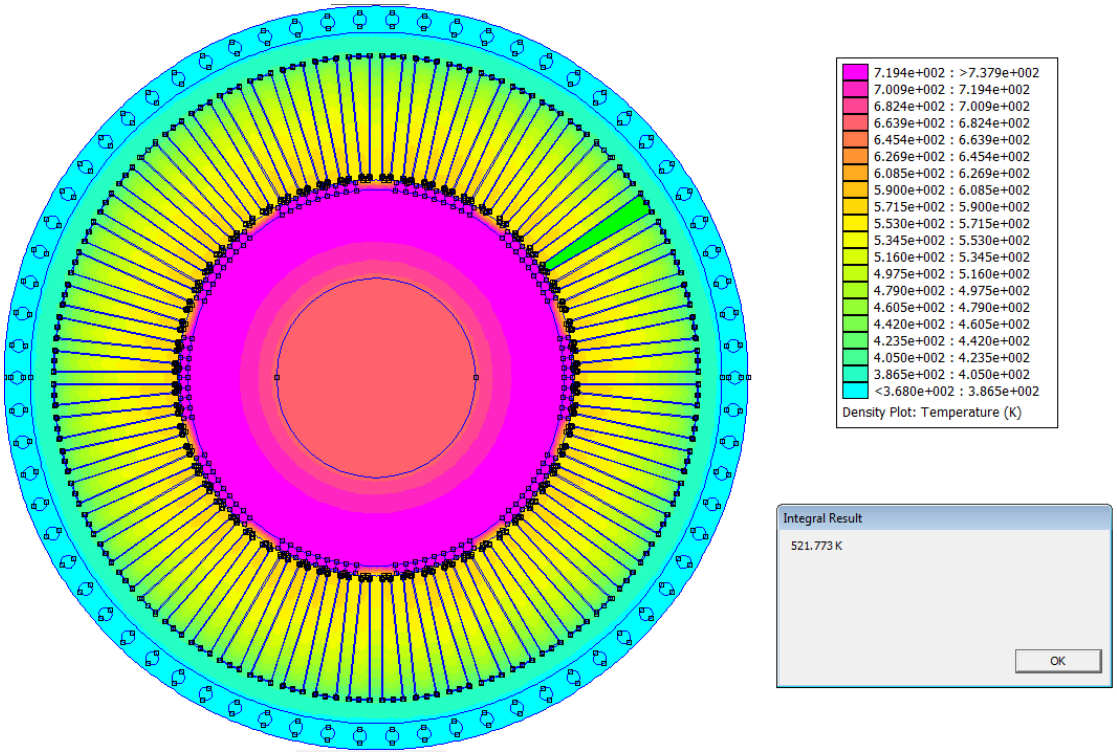

Figure 2.8.
Temperature distribution for the full scale configuration C, multiple test where run, none with acceptable winding temperatures.

2.3.4 Cooling MatLab VS Maxwell

In order to know how many cooling channels that could be allowed to be added in the MatLab model for it to be able to be transferred to the Maxwell model a quick test was conducted. This since the initial cooling channels in the MatLab code was circular and the cooling channels in Maxwell are rectangular. The assumption was made that the heat conduction on average on the cooling surface was the same.

Every cooling channel in MatLab will always be of the same size no matter the layout of the EM whereas the size of the cooling channel for Maxwell varies with the outer diameter of the EM. Initially three different tests were conducted one for each configuration. But since none of B or C can use their full size these where not of that much interest in the end. Instead configuration A became the benchmark of how many channels where allowed in MatLab.

When running the comparison between MatLab and Maxwell for configuration A it was discovered that for a 36 cooling channel Maxwell model, the maximum allowed number of cooling channels in MatLab was 70. Since the number of cooling channels in Maxwell is set to the same as the number of wiring slots for the sake of symmetry when it comes to simulations the area is actually bigger for most cases. 70 was therefore selected as standard since the heat transfer will be somewhat different in the 3D case as well.

2.4 Specification of models for electromagnetic design

2.4.1 Maxwell 2D

Maxwell 2D offers a step up from RMxprt, the model is still 2D but here a more detailed version of the machine can be created as well as a more precise analysis. This model is a bit more time consuming to run than the RMxprt, however the results are deemed to be far more representative of the actual machine. Here both time dependent loss distribution and magnetic flux can be visualized on the machine as well as acquiring time dependent loss and torque.

2.4.2 Maxwell 3D

Maxwell 3D takes the final step of converting the problem to a 3D case, this model is far more time consuming and should only be used when the 2D case has identified operational conditions that seems to be of interest. Just like the 2D version loss distribution and so on can be seen in this model with the added advantage of looking at the full 3D structure of the EM, as well as the winding coming out of the side of the generator.

2.5 Power loss modelling for electrical machines

Several studies have been made where the distribution of losses in generators have been investigated. Unfortunately the studies that has been used as reference during the writing of this paper could not be used as a benchmark for loss distribution due to the fact that these studies includes losses that are not present in the present design such as rotor winding losses among other things. Therefore no final conclusion can be taken regarding whether the loss distribution presented reflects what typically can be expected.

2.5.1 Losses in winding

The biggest loss in generators typically come from losses generated in the winding as a result of electricity traveling through it. These losses occur as a result of collisions between electrons as they are traveling through the conductor and can be calculated according to:

$$\mathrm{Pr} = I^2 R_{DC} = \frac{V^2}{R_{DC}} \qquad (2.7)$$

$$R_{DC} = \frac{\rho l}{A} \qquad (2.8)$$

Where l is the length of the conductor, A the cross-section area, I the current and ρ the material resistivity. The material resistivity is however not a constant but changes with temperature. This change can generally be described with the following equation:

$$\rho(T) = \rho(T_0)[1 + \alpha(T - T_0)] \qquad (2.9)$$

Where T_0 is the reference temperature and α the temperature coefficient of resistance. This is however not the only loss generated in the winding. As the frequency of the current goes up so does the losses as well, this is due to the skin effect. In simple terms the skin effect can be explained thusly: If the frequency increases the conductivity at the center of the winding decreases, the area still conducting electricity is referred to as "the skin". When the current density drops to a level below 0.368 of its original value it is no longer deemed to belong to the

skin area of the conductor. The depth of the skin can be expressed as a function of frequency according to:

$$\delta = \sqrt{\frac{\rho}{\pi f \mu_r \mu_0}} \qquad (2.10)$$

Where δ is the skin depth in m, f the frequency, μ_r the relative permeability and μ_0 the permeability of free space ($4\pi \times 10{-}7$ (H/m)) [11].

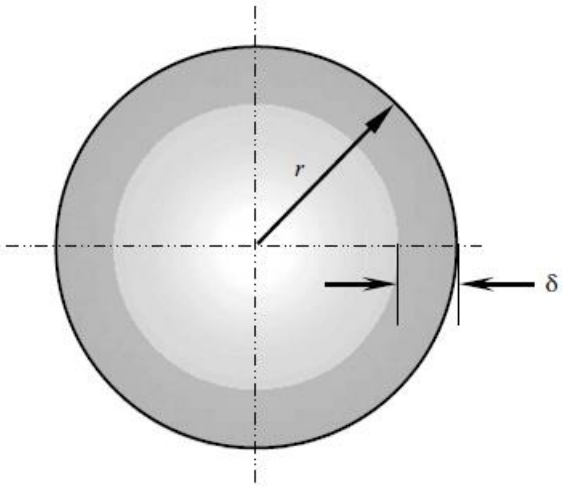

Figure 2.9.
Visualisation of skin depth, image taken from [9].

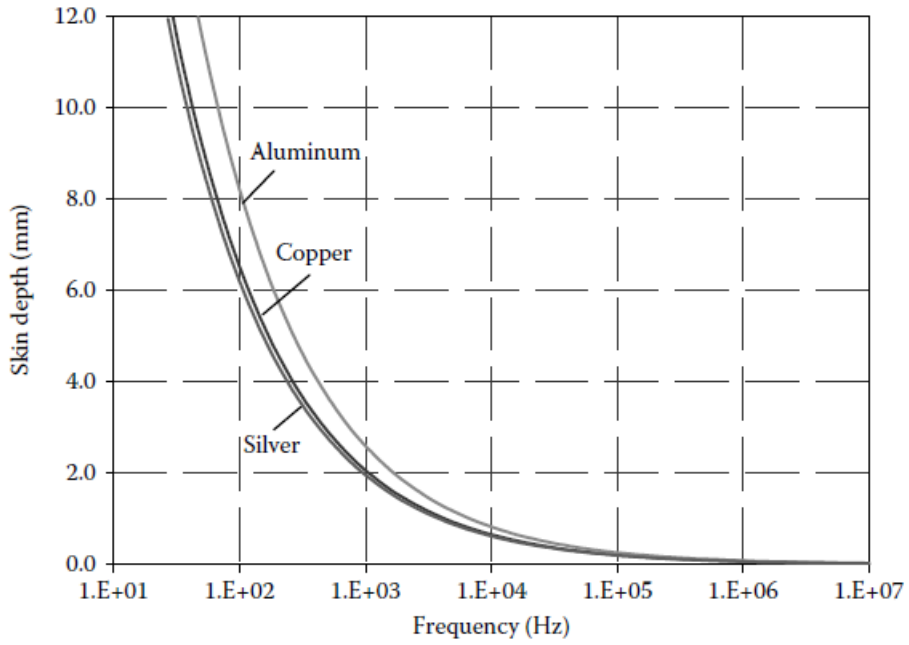

Figure 2.10.
Skin depth as a function of frequency, image taken from [9].

2.5.2 Eddy current losses

Eddy current losses can be explained by using Faraday's law, as the electrical flow in the windings changes direction so does the magnetic flux. This generates an electromagnetic field (EMF) which in turns generates circulating currents in bulk conductors in the magnetic field (the iron core) [11].

The only way to influence the losses due to eddy current is to alter the core itself. The most common way of limiting losses due to eddy currents are to divide up the core using stack lamination which in turn are insulated. This prevents the eddy currents from creating large loops which in turn results in smaller losses.

In short eddy current losses can be calculated with the equations below, for a more detailed explanation of where this expression comes from please see [11]. In equation (2.11) below eddy current losses (P_e) are calculated in watt in accordance to:

$$P_e = \frac{\pi^2}{6} V_c B^2 f^2 a^2 \sigma = K_e V_c B^2 f^2 \qquad (2.11)$$

$$K_e = \frac{\pi^2 a^2 \sigma}{6} \qquad (2.12)$$

Where V_c is the volume of the magnetic core in m^3, a the lamination thickness in m, σ is the electrical conductivity, f the magnetization frequency and B the magnetic peak flux density.

Eddy current losses also occurs in the magnets themself. These losses can be calculated using equations (2.13) and (2.14) below. The eddy current losses in the magnets (P_m) are here calculated in watt.

$$P_m = K_m V_m B^2 f^2 \qquad (2.13)$$

$$K_m = \frac{b_m^2}{12 \rho_m} \qquad (2.14)$$

Where b_m is the magnet width and ρ_m is the magnet resistivity ($\rho = 1/\sigma$) [11].

2.5.3 Hysteresis losses

Magnetic hysteresis losses occur in ferromagnetic materials, in this case the core. The ferromagnetic material in the core will always try to align its own atomic dipole structure in accordance with the surrounding magnetic field. However since the magnetic field always changes as a result of the rotating magnets in the rotor, the dipoles will always be in a changing state. However since the ferromagnetic material tends to retain some magnetization also known as hysteresis some energy will be needed in order to cancel out this magnetization, this is the hysteresis loss. These losses are dependent on a number of factors such as power frequency, peak flux density, the core material and the orientation of the magnetic flux in relation to the grain structure of the core material.

In short hysteresis losses can be calculated with the equations below, for a more detailed explanation of where this expression comes from please see [11]. In equation (2.15) below hysteresis losses (P_h) are calculated in watt in accordance to:

$$P_h = K_h V_c B^n f \qquad (2.15)$$

Where V_c is the volume of the magnetic core in m^3, K_h the hysteresis coefficient, n the Stenmetz coefficient (has a value between 1.6 and 2.3, usually around 2) and f the magnetization frequency.

A list of common values for the hysteresis coefficient can be found in table 2.8 below [11]. For more exact data on the material used in this paper see table 4.1 - 4.3.

Table 2.8.
Hysteresis coefficient for different materials.

Materials	Hysteresis Coefficient $K_h(J/m^3) \cdot 10^{-2}$
Cast iron	27.63 – 40.2
Sheet iron	10.05
Cast steel	7.54 – 30.14
Hard cast steel	63 – 70.34
Silicon steel (4.8% in Si)	1.91
Hard tungsten steel	145.7
Good dynamo sheet steel	5.02
Mild steel casting	7.54 – 2.61
Nickel	32.66 – 100.5
Permalloy	0.25

2.5.4 Excess losses

Excess eddy current losses or just excess losses as they are referred to sometimes are eddy losses not explained by the classical eddy loss model. They are believed by some to be the result of material thickness, cross-section area, and the conductivity. Others believe that they are the result of the nonlinear electromagnetic field diffusion in the lamination [15]. Since there is no conclusive formula for these losses they will simply be defined according to equation (2.16) below.

$$P_{core} = k_h B^2 f + K_c (Bf)^2 + K_e (Bf)^{3/2} \qquad (2.16)$$

Where K_h are the coefficient for hysteresis losses, K_c the coefficient for classical eddy-current losses, K_e the coefficient for excess eddy-current losses and B the peak flux density [11].

2.6 Specification of models for cooling circuits and heat dissipation

In order to see what kind of cooling conditions that can be expected for the boundary conditions a number of calculations where made both for the air flow and the oil flow. The proposed values for these during the different operating points can be found in table 2.10 and 2.13. This subchapter provides a more in depth explanation of how this conclusion was reached. For a clearer illustration of where these values would be used se figure 2.11 below.

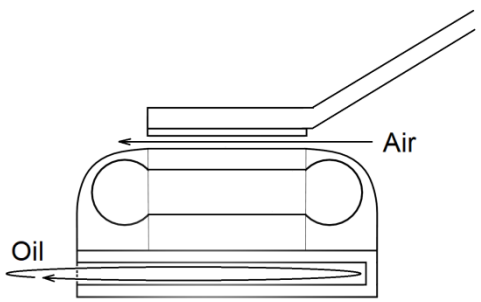

Figure 2.11.
Visualisation of where the boundary conditions ably.

2.6.1 Conduction

Conduction is the process of leading heat through a material. In this sub chapter the materials is assumed to be homogeneous, isentropic and the conductivity is assumed to be constant.

If one imagines a block of a material with heat conductivity λ, a thickness y and a temperature of T_1 on one side and T_2 on the other side (this does not necessarily need to be the same temperature as the surrounding) a one dimensional problem is acquired. Since we do not assume (in this example) that any heat is generated inside the body the temperature distribution should look as follows:

$$T = c_1 x + c_2 \qquad (2.17)$$

Where c_1 and c_2 are two constants and x is the position in the block with 0 representing the left side and y the right side.

The heat transfer for this block can be written as:

$$T_1 - T_2 = \frac{y}{\lambda A}\dot{Q} \qquad (2.18)$$

Where λ is the heat conduction, A the cross section area and $\dot{Q}$ the heat transfer rate. Adding several blocks after one another therefore gives the following expression [16].

$$T_1 - T_4 = \dot{Q}\left(\frac{y_1}{\lambda_1 A} + \frac{y_2}{\lambda_2 A} + \frac{y_3}{\lambda_3 A}\right) \qquad (2.19)$$

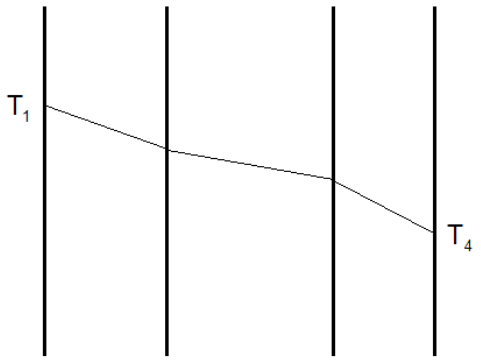

Figure 2.12.
Temperature distribution over three bodies due to their different properties.

2.6.2 Convection

When heat is transported between a fluid and a solid material this is known as convection. The heat transport in the fluid occurs due to molecular heat conduction and transport of internal energy due to the macroscopic motion of the fluid. In this case the conduction occurs as a result of oil moving over the cooling surface inside the generator, as well as air movement caused by a pressure gradient in the flow direction as well as the movement of the rotor perpendicular to this

motion, meaning that this is what's referred to as forced convection. The amount of heat that can be removed due to convection can be expressed as following:

$$Q/A = q \qquad (2.20)$$

Where Q is the total heat transfer, A the contact area and q hence the heat transfer per area. The value q can in turn be described as:

$$q = \alpha(t_w - t_f) \qquad (2.21)$$

Where α is the heat transfer coefficient, t_w the wall temperature and t_f the temperature of the flow. The heat transfer coefficient is however a non-constant dependent on several different factors such as the geometry of the body and properties of the fluid among other things [16]. For a more detailed description of how this phenomenon works it is recommended to read [16], in this paper however no deeper explanation will be given due to the complexity of the area.

In this machine there is as mentioned both convection with oil and air. Initially calculations are conducted to look at the heat transfer coefficient for the oil which can be assumed to have a temperature of 368 K. Initial values for the oil is taken from [17] where the assumption is made that the oil that is used have similar properties to "SAE 15W-40".

Based on [5] the cooling capacity per kg/s oil is 13.5 kW, in order to make sure that the system is not under dimensioned a safety factor of two is used. As well as the assumption that 10 % of the available cooling capacity is lost due to absorption of heat along the cooling system.

Table 2.9.
Data for SAE 15W-40 oil at diferent temperatures.

Temp. [°C]	Dyn. Viscosity $[\boldsymbol{kg/(m \cdot s)}]$	Kin. Viscosity $[\boldsymbol{m^2/s}]$	Density [kg/m³]
0	1.3280	$1489.4 \cdot 10^{-6}$	891.6
10	0.58295	$658.60 \cdot 10^{-6}$	885.1
20	0.28723	$326.87 \cdot 10^{-6}$	878.7
30	0.15531	$178.01 \cdot 10^{-6}$	872.5
40	0.091057	$105.10 \cdot 10^{-6}$	866.3
50	0.057172	$66.464 \cdot 10^{-6}$	860.2
60	0.038071	$44.585 \cdot 10^{-6}$	853.9
70	0.026576	$31.350 \cdot 10^{-6}$	847.7
80	0.019358	$23.006 \cdot 10^{-6}$	841.4
90	0.014588	$17.467 \cdot 10^{-6}$	835.2
100	0.011316	$13.648 \cdot 10^{-6}$	829.1

From these data a polyfit is made in MatLab. Other data is taken from [18] where "SAE 15W-40" is looked at as a "*Group II Oil*" (conventional mineral oil-based diesel engine lubricant).

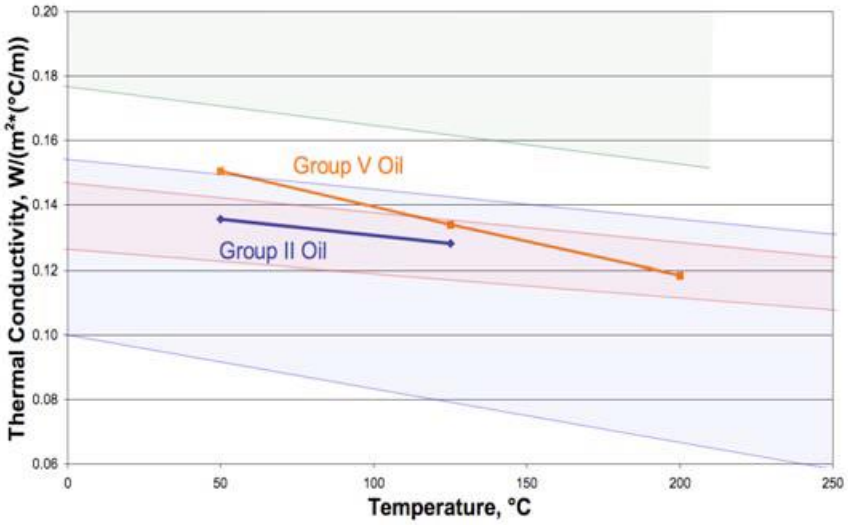

Figure 2.13.
Thermal conductivity of oil as a function of temperature, figure taken from [18].

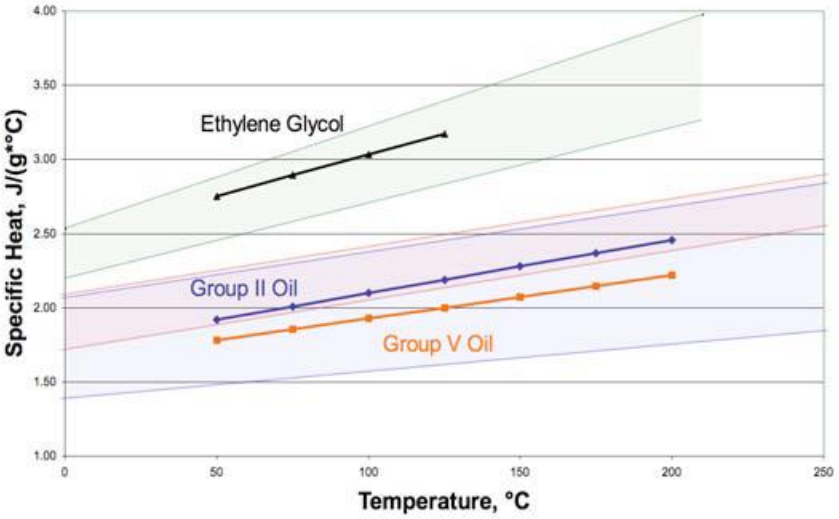

Figure 2.14.
Specific heat of oil as a function of temperature, figure taken from [18].

Once this is done the calculations for acquiring the heat transfer coefficient can start. First is the Prandtl number which is given by equation (2.22) is calculated [16].

$$\mathrm{Pr} = \frac{\nu \rho c_p}{\lambda} = \frac{\mu c_p}{\lambda} \qquad (2.22)$$

Where v is the kinematic viscosity, ρ the density, μ the dynamic viscosity, c_p the specific heat and λ the thermal conductivity.

After the Prandtl number is calculated the hydraulic diameter of the flow channel as well as the speed of the flow is needed. The flow area is set to have an inner and outer diameter of 205 and 255 mm respectively, and 25 % of the available area in this cross section is used as flow area for either direction. Combined with previously listed data and assuming that the oil has a temperature of 95 °**C** flow speeds can be calculated. In order to get a hydraulic diameter D_h, the correlation in figure 2.15 is used, based on the assumption that the wall temperature can be seen as constant [16].

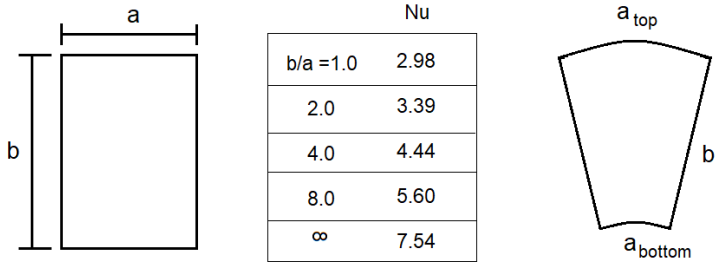

Figure 2.15.
Nusselt number as a function of b/a ratio.

In this picture the "a" value is assumed to be an average value of the "a" in the top and "a" in the bottom giving a b/a ratio of 2.4911. Now the Reynolds number can be calculated for the cross section followed by the Nusselt number [16].

$$Re_D = \frac{u_m D}{v} \qquad (2.23)$$

Where u_m is the flow velocity of the oil and D is the hydraulic diameter of the channel.

$$Nu_D = 3.656 + \frac{0.0668 Re_D PrD/x}{1 + 0.04(Re_D PrD/x)^{2/3}} \qquad (2.24)$$

Lastly the value of interest can be calculated the oil heat transfer coefficient α which was found to be in accordance with table 2.10 [16].

$$\alpha = \frac{Nu_D \lambda}{D} \qquad (2.25)$$

Table 2.10.
Heat transfer coefficient $[w/m^2 \cdot K]$ for the oil at different operation points for the A, 10p 60sl (5) out-runner.

	1500 rpm	2200 rpm	6744 rpm	7362 rpm	7454 rpm
400 Amp	138.0579	142.4926	172.0103	175.9813	176.6170
500 Amp	149.2920	153.4333	180.9998	184.8634	185.4115

Once all of this is done the heat transfer coefficient for the air is calculated as well. Since the air property varies with operational conditions this calculation will be done five times, one for each operation point. It should nevertheless be mentioned that the air pressure of the flow is set to ambient when it should be higher. This calculation does not however take altitude into consideration and should therefore only be used as a test of concept. Initially the thermal conductivity is calculated using equation (2.26) from [19].

$$\lambda_{air} = (33.9729025 \cdot Tr^{-1}) + \left(-164.702679 \cdot Tr^{(-2/3)}\right) + \left(262.108546 \cdot Tr^{(-1/3)}\right) - 21.5346955 + \left(-443.455815 \cdot Tr^{(1/3)}\right) + \left(607.339582 \cdot Tr^{(2/3)}\right) + (-368.790121 \cdot Tr) + \left(111.296674 \cdot Tr^{(4/3)}\right) + (-13.4122465 \cdot Tr^{(5/3)}) \qquad (2.26)$$

Where

$$Tr = Temp_{air} \,/\, tc \qquad (2.27)$$

$$tc = 132.52 \qquad (2.28)$$

The next value to be calculated is the C_p value for the air based on data from [20].

Table 2.11.
Cp values for air at different temperatures.

Temp [K]	$C_{p\,air}\ [kJ/kg \cdot K]$
250	1.003
300	1.005
350	1.008
400	1.013
450	1.020
500	1.029
550	1.040
600	1.051

Once this is done the dynamic viscosity is calculated according to equation (2.29) [16] as well as air density according to equation (2.30) [21].

$$\mu = 0.01827 \cdot \left(\frac{0.555 \cdot 524.07 + 120}{0.555 \cdot T \cdot 1.8 + 120}\right) \cdot \left(\frac{T \cdot 1.8}{524.07}\right)^{3/2} \qquad (2.29)$$

$$\rho = \frac{P}{R_{air}T} \qquad (2.30)$$

Where T is the temperature, ρ the density, P the pressure and R_{air} the air gas constant ($287\ [J/kg \cdot K]$).

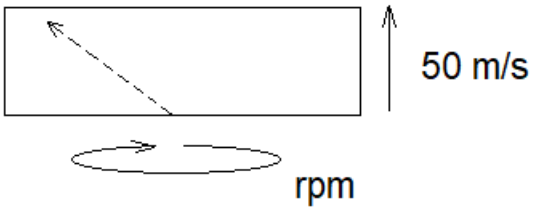

Figure 2.16.
Relative movement of the air along the outside of the generator as a result of the rotation.

The flow along the outside of the generator can be seen as a flow along a flat surface. The time it takes for the air to pass the generators is 0.0011s for an assumed speed of 50 m/s over a surface 0.055 m wide. Combined with the rotational speed the air travels at a **relative speed** along a distance equal to **distance travelled** according to table 2.12 below.

Table 2.12.
Movement properties for the air traveling alongside the rotor of the generator.

	Relative speed [m/s]	**Distance travelled [m]**
1500 rpm	61.2301	0.0674
2200 rpm	72.0208	0.0792
6744 rpm	166.5826	0.1832
7362 rpm	180.5254	0.1986
7454 rpm	182.6093	0.2009

After this the Prandtl number is calculated using equation 2.22. Followed by the Reynolds number for the air according to equation (2.31) as well as the kinematic viscosity (2.32) [16].

$$Re = \frac{U_0 L}{v} \qquad (2.31)$$

Where U_0 is the relative speed and L the distance travelled.

$$v = \frac{\mu}{\rho} \qquad (2.32)$$

After this the Nusselt number is calculated according to equation (2.33) if the Reynolds value is below $5 \cdot 10^5$ or (2.34) if it is between $5 \cdot 10^5$ and $1 \cdot 10^7$(no values where above this limit). Once this is done the shear stress coefficient C_F is calculated according to equation (2.35) [16].

$$Nu = 0.664 \cdot \sqrt{Re} \cdot Pr^{1/3} \qquad (2.33)$$

$$Nu = 0.37 Pr^{1/3} (Re^{4/5} - 23550) \qquad (2.34)$$

$$C_F = \frac{2 \cdot Nu}{Re \cdot Pr^{1/3}} \qquad (2.35)$$

And finally the heat transfer coefficient is calculated with equation (2.36) [16].

$$\alpha = \frac{C_F \cdot \rho \cdot c_p \cdot U}{2} \qquad (2.36)$$

From this the following values are obtained.

Table 2.13.
Heat transfer coefficient along the outside of the rotor at different rotational speeds for the A, 10p 60sl (5) out-runner.

	Heat transfer coefficient α $[W/m^2K]$
1500 rpm	93.8918
2200 rpm	93.8918
6744 rpm	46.2037
7362 rpm	45.7195
7454 rpm	50.3743

2.7 Specification of models for heat transfer analysis

In this subchapter models that will utilize the boundary conditions calculated in chapter 2.6 are presented.

2.7.1 MatLab FEMM (thermal)

The goal here was to use the MatLab and FEMM tool combination mentioned earlier in chapter 2 since this would allow for a thermal analysis of the problem. The initial idea was to rework the MatLab code so that it only looks at the thermal aspects of the problem and changing the layout so that it looks at the out-runner case at hand. It would then be possible to analyze the thermal problem by setting the inputs so they reflect the simulations run in Maxwell. The losses would now be distributed manually over different regions of the generator. The exact distribution might be slightly incorrect since it is completed by hand, but the total value of these losses can then scaled so that they are the same as the Rms values for total losses calculated in Maxwell. Unfortunately this code was never completed so no detailed analysis of this problem was ever performed.

3 Evaluation of different machine configurations

In this chapter results from different early models can be found, as well as evaluations regarding which of these that show promise and will be investigated further. The process used in this paper for evaluating what configuration and layout that should be used can be visualized according to figure 3.1.

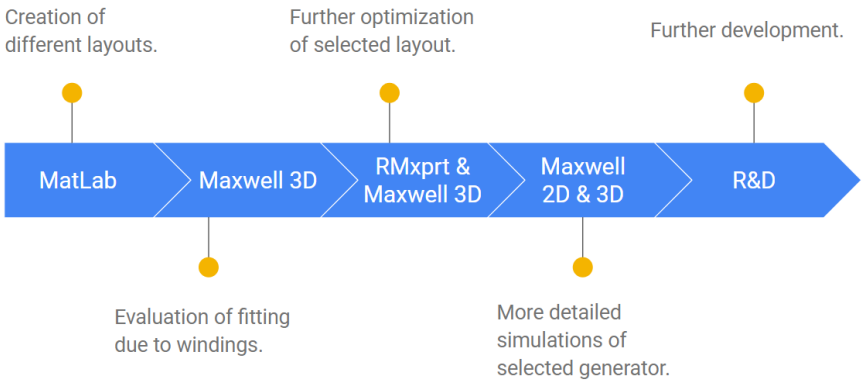

Figure 3.1.
Conceptual development proces.

3.1 Conceptual design

From equation (2.5) and (2.6) the following data is acquired based on the assumption that the shear stress σ is 20,7 kN/m^2 and a speed of 6744 rpm.

Table 3.1.
Estimated torque and power output for the three configurations based on equation (2.1) and (2.2).

Configuration	l [mm]	r_{rotor} [mm]	Torque [Nm]	Power [kW]
A	150	150	438.96	309.98
B	95	270	900.74	636.09
C	135	150	395.06	278.98

Not much can be said about these values on their own, except that reaching the required power levels for the different configurations does not seem to be much of a problem.

3.2 MatLab design

In order to get an initial understanding of the optimal design for the generator numerous numerical experiments were run in MatLab. From these it was concluded that the most promising generator was the A configuration 10p 60sl (5). This subchapter provides a more in depth explanation of how this conclusion was reached.

Initially numerous tests where done in order to decide the final dimensional parameters for the EM, but eventually the most important factor was found to be the size of the slots. In the 2D cases it is hard to get an understanding of how big the slots can be allowed to be since these models do not take in to account the amount of winding coming out of the sides of the generator. However by using Maxwell 3D an approximation of this width was given.

Numerous different varieties for each configuration were run, the results of these tests can be found below. As can be seen configuration A was the configuration that was the most appropriate since the others simply had too much winding sticking out to be of interest.

The results produced in MatLab are however not deemed to be very accurate when it comes to the machines behavior. Instead it should more be taken as an indication of where the most advantageous design can be found, in terms of configuration layout.

Table 3.2.
Input data for MatLab simulation.

Configuration	Outer radius of stator core	Relative inner radius for the machine	Relative width of machine	Slotting factor	Gap radius factor
A, 10p 60sl	200 mm	0.5	0.75	0.5	0.85
A, 8p 48sl	200 mm	0.5	0.75	0.6	0.85
B, 8p 48sl	350 mm	0.61429	0.27143	0.4	0.7
C, 8p 48sl	250 mm	0.38	0.54	0.35	0.7
C, 6p 36sl	270 mm	0.34545	0.5	0.33	0.7

Table 3.3.
Width for the different machine configurations and layouts.

Machine configuration	Total allowed width	Total width off wiring	Remaining width of machine
A, 10p 60sl	150 mm	152 mm	-2 mm
A, 8p 48sl	150 mm	180 mm	-30 mm
B, 8p 48sl	95 mm	172 mm	-77 mm
C, 8p 48sl	135 mm	164 mm	-29 mm
C, 6p 36sl	135 mm	188 mm	-53 mm

The results of the initial tests shown above points towards that the configuration most likely to fit inside the compressor housing would be the 10 pole 60 slot configuration A. But in order to have something to compare with the 8 pole 48 slot version of configuration A and C will also be tested further.

Table 3.4.
Input data for MatLab simulation.

Configuration	Outer radius of stator core	Relative inner radius for the machine	Relative width of machine	Slotting factor	Gap radius factor
A, 10p 60sl (1)	200 mm	0.5	0.75	0.5	0.6
A, 10p 60sl (2)	200 mm	0.5	0.75	0.45	0.6
A, 10p 60sl (3)	200 mm	0.5	0.75	0.44	0.66
A, 10p 60sl (4)	200 mm	0.5	0.75	0.4	0.6
A, 10p 60sl (5)	200 mm	0.5	0.75	0.35	0.6

Table 3.5.
With of machine according to Maxwell.

Machine configuration	Total allowed width	Total width off winding	Remaining width of machine	Predicted output
A, 10p 60sl (1)	150 mm	120 mm	30 mm	58.1 kW
A, 10p 60sl (2)	150 mm	110 mm	40 mm	69.95 kW
A, 10p 60sl (3)	150 mm	120 mm	30 mm	57.5 kW
A, 10p 60sl (4)	150 mm	103 mm	47 mm	71.75 kW
A, 10p 60sl (5)	150 mm	95 mm	55 mm	71.24 kW

As can be seen above it was possible to decrease the size of the windings for configuration A significantly by changing the layout of the generator.

Table 3.6.
Input data for MatLab simulation.

Configuration	Outer radius of stator core	Relative inner radius for the machine	Relative width of machine	Slotting factor	Gap radius factor
A, 8p 48sl (1)	200 mm	0.5	0.75	0.5	0.6
A, 8p 48sl (2)	200 mm	0.5	0.75	0.45	0.6
A, 8p 48sl (3)	200 mm	0.5	0.75	0.4	0.6
A, 8p 48sl (4)	200 mm	0.5	0.75	0.35	0.6
A, 8p 48sl (5)	200 mm	0.5	0.75	0.5	0.55
A, 8p 48sl (6)	200 mm	0.5	0.75	0.45	0.55
A, 8p 48sl (7)	200 mm	0.5	0.75	0.4	0.55
A, 8p 48sl (8)	200 mm	0.5	0.75	0.35	0.55

Table 3.7.
With of machine according to Maxwell.

Machine configuration	Total allowed width	Total width off winding	Remaining width of machine	Predicted output
A, 8p 48sl (1)	150 mm	126 mm	24 mm	43.5 kW
A, 8p 48sl (2)	150 mm	114 mm	36 mm	56.5 kW
A, 8p 48sl (3)	150 mm	106 mm	44 mm	61.2 kW
A, 8p 48sl (4)	150 mm	96 mm	54 mm	62.7 kW
A, 8p 48sl (5)	150 mm	118 mm	32 mm	52 kW
A, 8p 48sl (6)	150 mm	108 mm	42 mm	58 kW
A, 8p 48sl (7)	150 mm	97 mm	53 mm	62.2 kW
A, 8p 48sl (8)	150 mm	88 mm	62 mm	59.5 kW

By changing the layout of the 8 pole 48 slot configuration A it was possible to decrease the width of this machine as well however not enough to make it more power dense then the 10 pole 60 slot version.

Finally there is the 8 pole 48 slot C configuration, this machine however was not as successful in its resizing effort. For this reason no detailed data for this version was compiled.

In order to decide which layout among the 10 pole 60 slot configuration A that will be the base for the more in depth analysis a number of simulations where run using Maxwell RMxprt. The result from these can be found in figure 3.2 below. The result from this however indicated that the most promising version of the generator is **A, 10p 60sl (5)**.

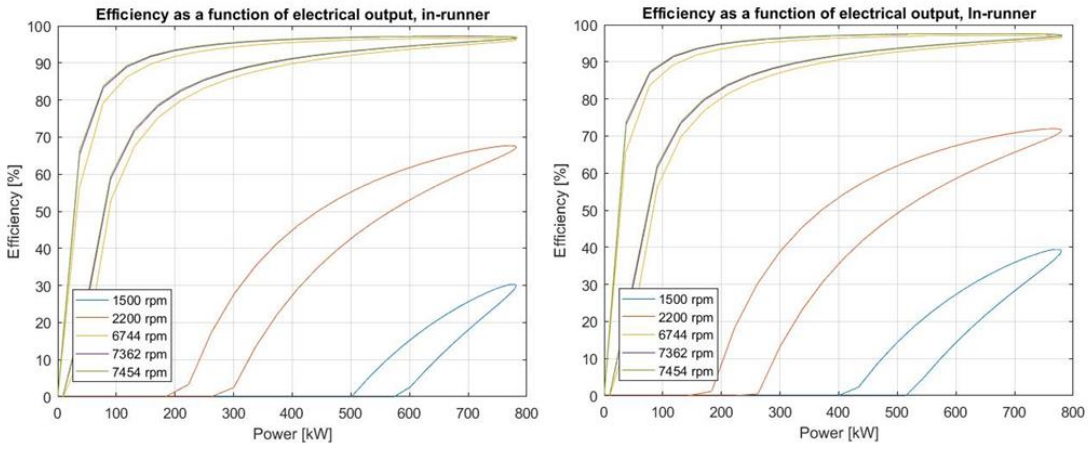

Figure 3.2.
In this figure output data according to RMxprt can be found for configuration A,10p 60sl (4) in-runner to the left and A,10p 60sl (5) in-runner to the right.

3.3 Comparison between inner and outer rotor machine

Once the most promising configuration and layout was chosen (A, 10p 60sl (5)) one final choice remained, the choice between an in-runner or out-runner configuration. As mentioned in the introduction chapter an out-runner configuration can utilize a higher speed due to more outer placement of the rotor. For a better understanding of the conceptual difference between an in-runner and an out-runner see figure 3.3.

In order to get an idea of the difference in configuration, the generator in question was modified in to an out-runner without changing the size of the slot and maintaining a similar placement of the wiring in radial direction. The initial results of these numerical experiments can be seen in graphs in figure 3.4 below. According to these tests **the out-runner is better** both when it comes to efficiency at low rpm as well as offering a larger power output than the in-runner. Another big favor for the out-runner is the lower current traveling through the wiring since large currents generates large losses.

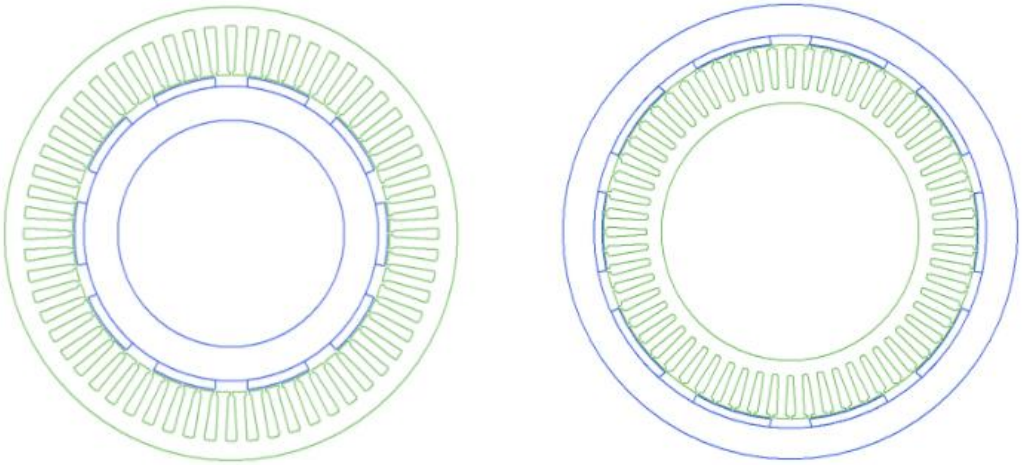

Figure 3.3.
Conceptual difference between an in-runner generator on the left (rotor on the inside and stator on the outside) and an out-runner on the right (rotor on the outside and stator on the inside)

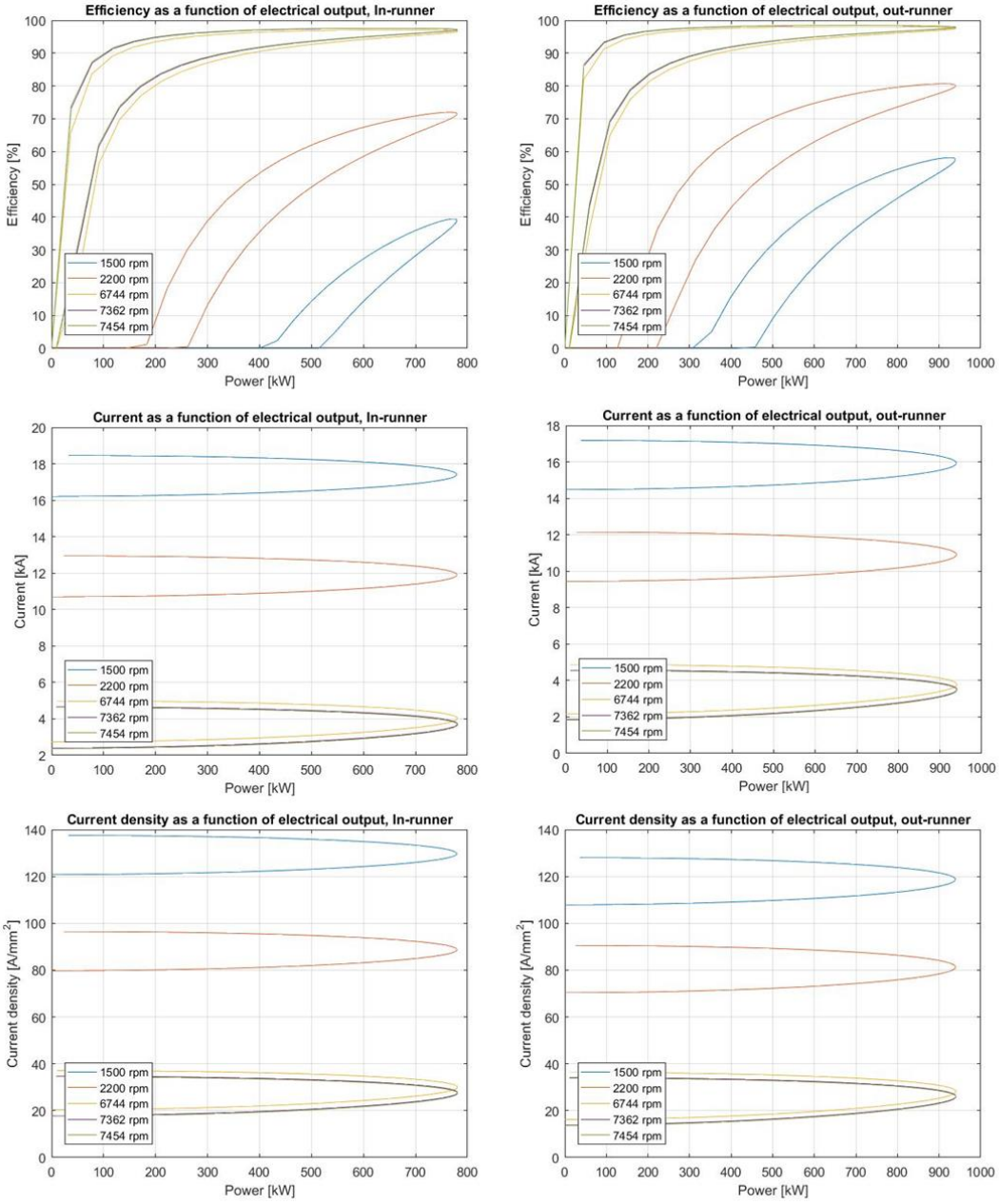

Figure 3.4.
RMxprt data from configuration A 10p 60sl (5), to the left the In-runner version and to the right the Out-runner.

4 Advanced design

After deciding what layout to utilize for the machine all that remains now is to run a more detailed analysis to get a more accurate prediction of the generators behaviour. The following material settings have been used for all simulations in this chapter.

Table 4.1.
Material properties for M250-35A (stator core).

Name	Type	Value	Units
Relative Permeability	Nonlinear	See table 4.2	
Bulk Conductivity	Simple	0	Siemens/m
Magnetic Coercivity	Vector		
- Magnitude	Vector Mag	0	A_per_meter
- X Component	Unit Vector	1	
- Y Component	Unit Vector	0	
- Z Component	Unit Vector	0	
Core Loss Model		Electrical Steel	W/m^3
- Kh	Simple	166.605376674989	
- Kc	Simple	0.366335041357434	
- Ke	Simple	0.0773000659968	
- Kdc	Simple	0	
Mass Density	Simple	7650	kg/m^3
Composition		Lamination	
- Stacking Factor	Simple	0.97	
- Stacking Direction		V(3)	
Young's Modulus	Simple	0	N/m^2
Poisson's Ratio	Simple	0	
Magnetostriction	Custom	None	
Inverse Magnetostriction	Custom	None	

Table 4.2.
Relative permeability input for M250-35A. The relative permeability B (Tesla) is the magnetic flux as a result of H (ampere per meter).

Nr	H (A_per_meter)	B (Tesla)
1	0	0
2	26.8	0.1
3	35.7	0.2
4	41.8	0.3
5	47.5	0.4
6	53.4	0.5
7	60	0.6
8	67.9	0.7
9	77.5	0.8
10	90	0.9
11	107	1
12	133	1.1
13	179	1.2
14	284	1.3
15	642	1.4
16	1810	1.5
17	4030	1.6
18	7290	1.7
19	11700	1.8
20	966630	1.9

Table 4.3.
Material properties for N33EH100degC (magnets).

Name	Type	Value	Units
Relative Permeability	Simple	1.062931	
Bulk Conductivity	Simple	555000	Siemens/m
Magnetic Coercivity	Vector		
- Magnitude	Vector Mag	-771120	A_per_meter
- X Component	Unit Vector	1	
- Y Component	Unit Vector	0	
- Z Component	Unit Vector	0	
Core Loss Model		None	W/m^3

Mass Density	Simple	0	kg/m^3
Composition		Solid	
Young's Modulus	Simple	0	N/m^2
Poisson's Ratio	Simple	0	
Magnetostriction	Custom	None	
Inverse Magnetostriction	Custom	None	

4.1 Maxwell 2D

In this subchapter a closer look was taken at the A, 10p 60sl (5) out-runner. It was concluded the A, 10p 60sl (5) out-runner would not be powerful enough to cover the power need for the airplane. Instead further simulations where run, here it was concluded that the A, 10p 60sl (5) out-runner would be replaced with a 12 pole 72 slot out-runner configuration instead. Data for this EM can be found in figure 4.6, this subchapter provides a more in depth explanation of how this conclusion was reached.

First up is the Maxwell 2D tool, after replicating the layout of the A, 10p 60sl (5) out-runner. The first task was to find what number of conductors that should be used to achieve a voltage rating of 400/230V. Since this value is also dependent on both the rotational speed of the engine and the current going through the wiring the speed will be set to cruise operations (6744 rpm) and the current will be a variable initially. Once the number of conductors is decided operations at different rpm will be run according to table 4.4 below, this in order to get a better understanding at different operating points for the machine.

Table 4.4.
Operations listing.

rpm\Amp	100	200	300	400	500
1500					
2200					
6744					
7362					
7454					

From these tests it was concluded that the final design of the generator will utilize 3 conductors, this to achieve a peak voltage rating of between 371 to 410 volt at 6744 rpm. The most troubling operation conditions are the ones at low rpms, this since the voltage rating takes a considerable dip compared to the high rpm voltage. A possible fix for these conditions would be to utilize some sort of power electronics, however some sort of regulating unit like the GCU will most likely be needed due to the varying voltage overall.

Table 4.5.
Maxwell 2D output data for a rotational speed of 6744 rpm.

	Torque [Nm]	Power [kW]	Losses [kW]	Efficiency [%]	Peak voltage [V]	RMS voltage [V]
100Amp	109	77.3	1.89	97.6	371	214
200Amp	212	150	1.9	98.7	381	220
300Amp	305	216	2.05	99.1	387	224
400Amp	388	274	2.4	99.1	395	228
500Amp	461	325	2.92	99.1	410	237

Table 4.6.
Maxwell 2D losses for a rotational speed of 6744 rpm.

	Eddy losses [W]	Excess losses [W]	Hysteresis losses [W]	Stranded losses [W]	Total losses [W]
100Amp	1380	6.79	463	40.4	1890.19
200Amp	1240	6.55	490	162	1898.55
300Amp	1170	6.49	511	363	2050.49
400Amp	1220	6.72	529	646	2401.72
500Amp	1360	7.15	544	1010	2921.15

The values in the tables above are all based on Rms values for the suggested generator at a speed of 6744 rpm. In the graph below a distribution of the losses in comparison to the total loss is done, from this it can be seen that the winding losses are a growing loss compared to the rest that get a smaller and smaller role as the current increases.

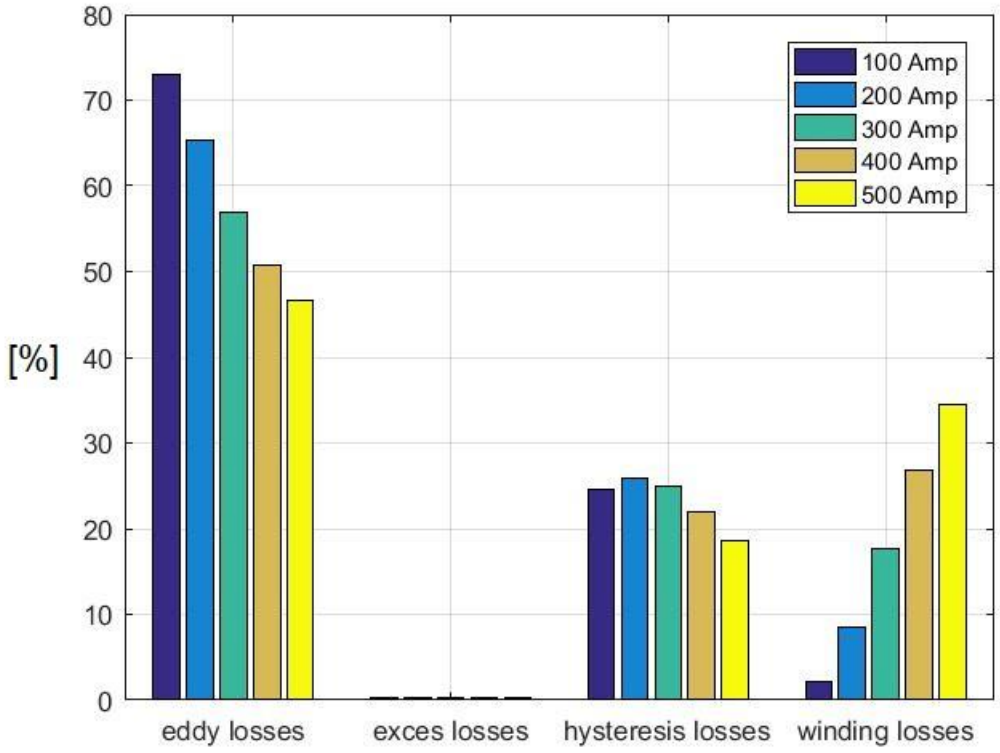

Figure 4.1.
Loss distribution for the EM at different currents for an operational speed of 6744 rpm.

Unlike the predictions however the largest losses (for the operations point investigated here) are not the winding losses but rather the eddy current losses. This may nevertheless be due to the fact that the machine is not operating at its maximum capacity if one looks at the RMxprt predictions.

In order to test the behaviour of the generator at a higher current a test at 1000 Amp was also made. The results from this simulation showed as suspected that the winding losses where now the biggest loss as can be seen in figure 4.2. The simulation also showed that the voltage curve was now almost unrecognisable as a sinus curve as can be seen in figure 4.3. Overall behaviour for the EM at 1000 Amp can be found in table 4.7.

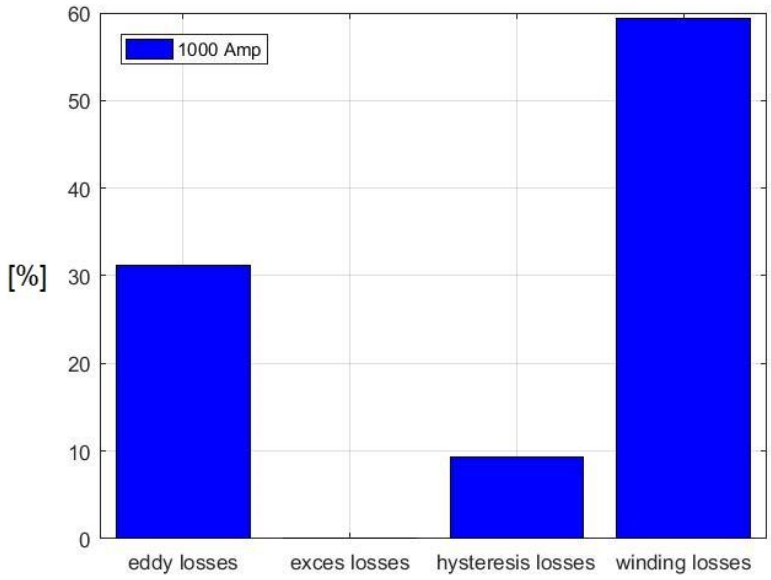

Figure 4.2.
Loss distribution for the EM during operations at 6744 rpm and 1000 Amp.

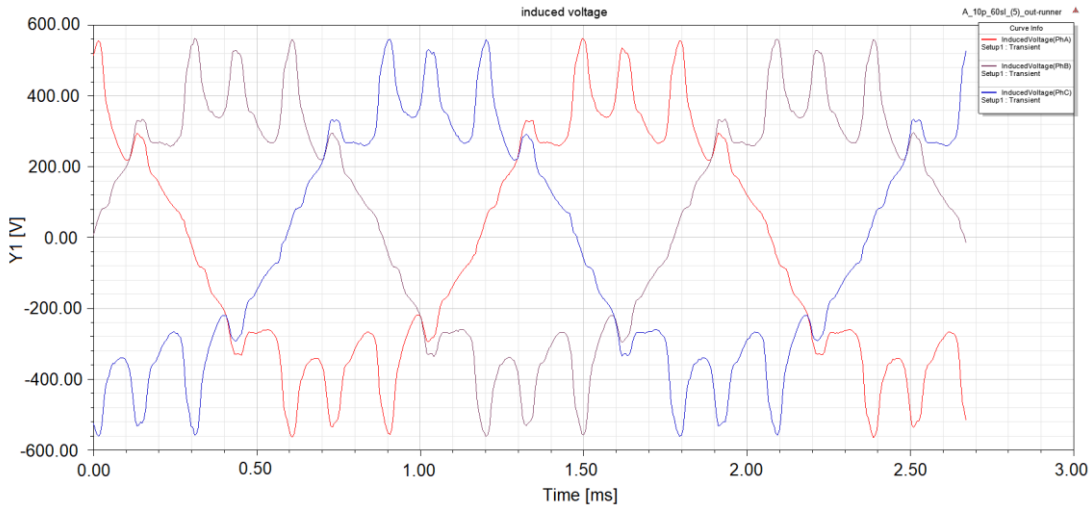

Figure 4.3.
Induced voltage for configuration A 10p 60sl (5) out-runner att 6744 rpm and 1000Amp.

	Torque [Nm]	Power [kW]	Losses [kW]	Efficiency [%]	Peak voltage [V]	RMS voltage [V]
1000Amp	712	503	6.8	98.6	561	397

Table 4.7.
Operational behaviour for configuration A 10p 60sl (5) out-runner at 6744 rpm and 1000 Amp.

Until now all results have been gained from a model without the housing structure responsible for cooling, However when adding this part no larger difference were found in the overall behaviour. To sum up the overall performance of the generator (with housing) the following figure can be used.

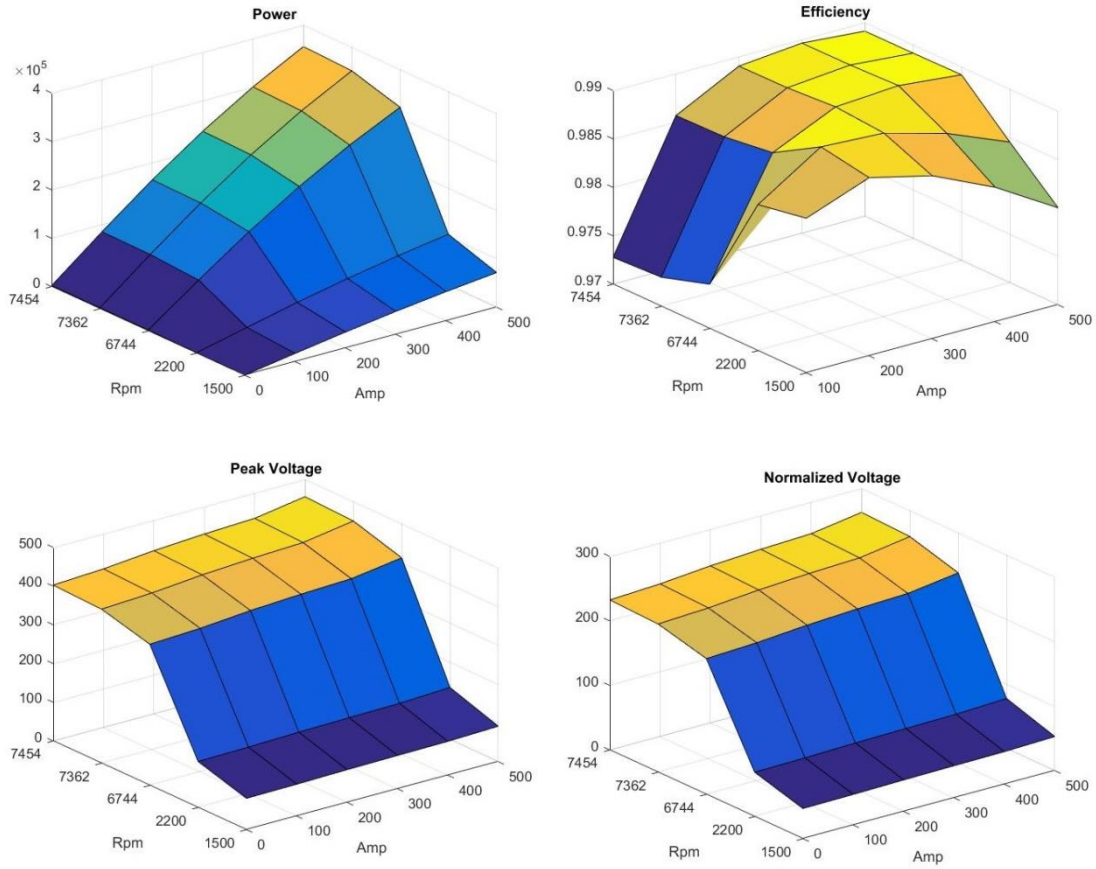

Figure 4.4.
Overall performance and voltage characteristics for the proposed EM.

This original configuration did however not offer enough power at low rpms to cover the power need on its own see table 4.8. So in order to cover this need two new generator configurations where tested, the first one was simply an extended version of the original, this one with a "core" with of 95 mm instead of the original 55 mm. Data for this configuration can be found in figure 4.4. The second one was a new 12 pole 72 slots configuration. Operational data from this configuration can be found in figure 4.5.

Table 4.8.
Power needed vs power delivered at different rpms for configuration A 10p 60sl (5) out-runner.
** for 1500 and 2200 rpm the maximum delivered power was used as "Power delivered", these values are taken from operations at 500 Amp.*

rpm	Power needed	Power delivered
1500	123 kW	72.4 kW
2200	123 kW	106 kW
6744	123 kW	123 kW
7362	156.6 kW	156.6 kW
7454	123 kW	123 kW

It should also be mentioned that at this point the operating rpm was changed somewhat in accordance with what can be seen in table 4.9 below, this was done by GKN.

Table 4.9.
New operating rpms for the generator.

Operation point	Old rpm value	New rpm value
Ground idle	1500	1500
Ground idle	2200	2200
Cruise	6744	6261
MTO	7362	6797
TOC	7454	6991

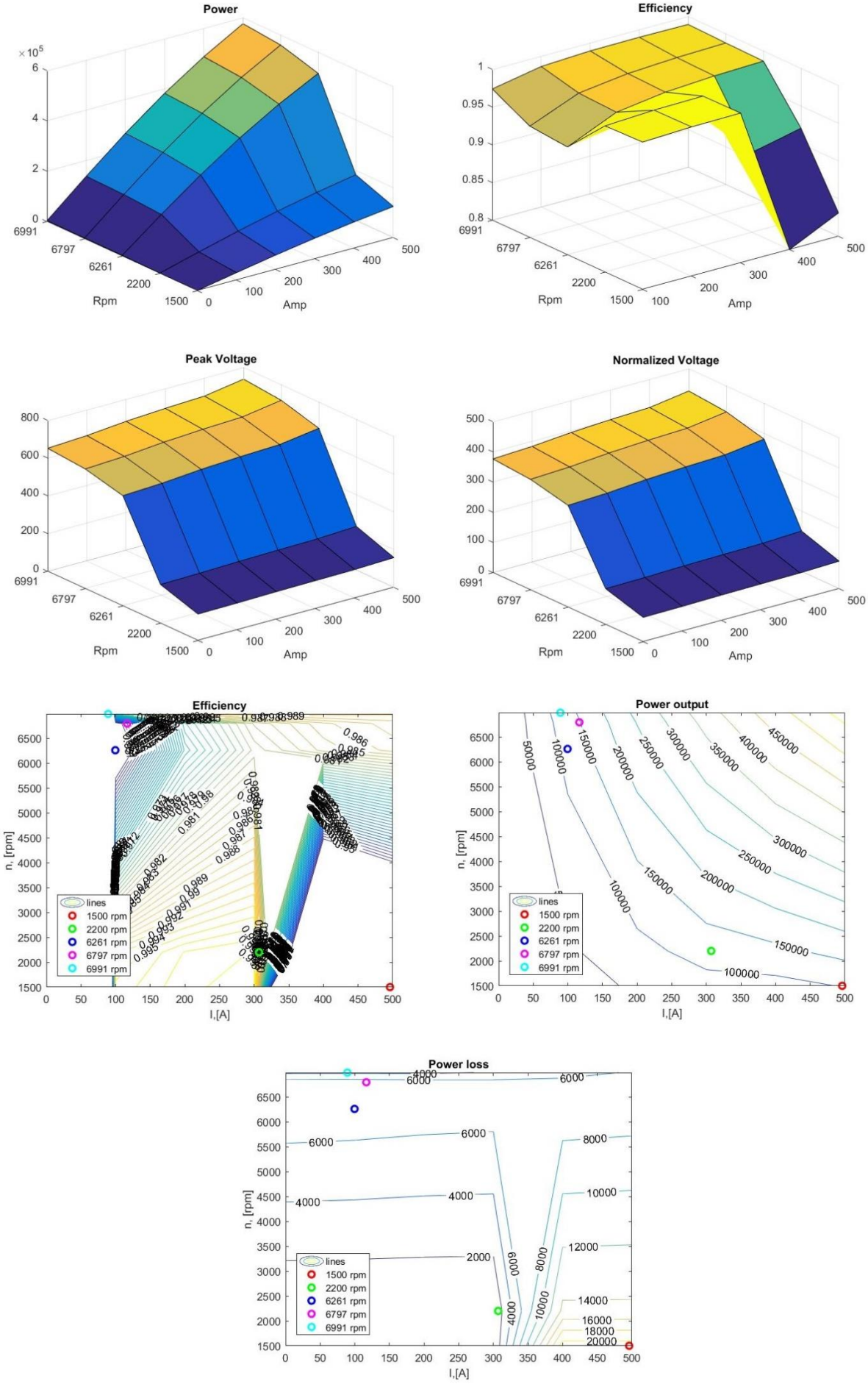

Figure 4.5.
Predicted behaviour of the extended 10 pole 60 slot generator.

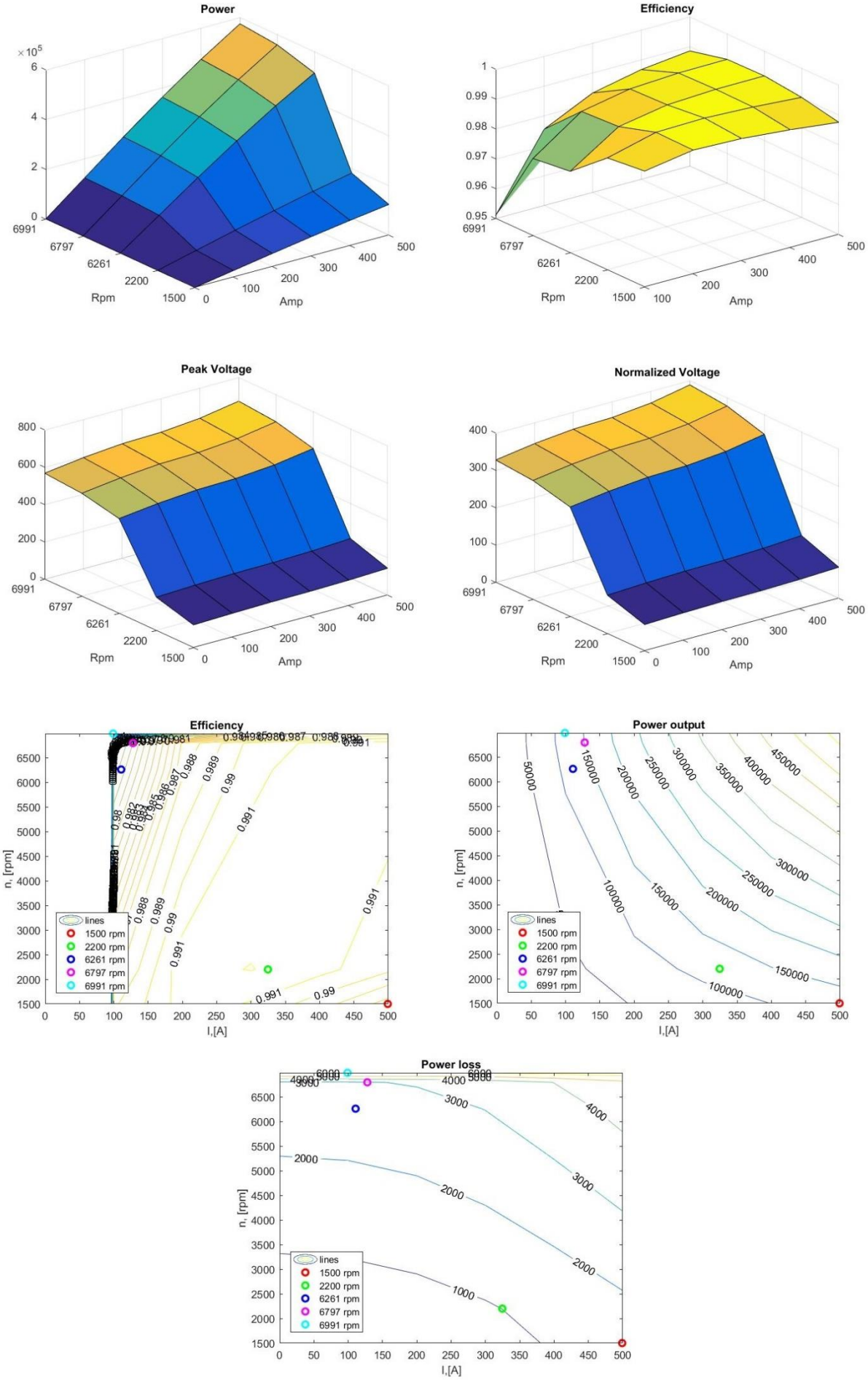

Figure 4.6.
Predicted behaviour of 12 pole 72 slot generator.

In order to have a good base for choosing what configuration to be used in the end a summary table was created (table 4.10) which can be found below.

Table 4.10.
Summary table of the tree configurations of interest.

	10p 60sl	**10p 60sl long**	**12p 72sl**
Weight	51.51 kg	82.30 kg	88.37 kg
Size	Ok	Unclear	Ok
Max Frequency	582 Hz	582 Hz	699 Hz
Needed Power	No	Yes	Yes
Max Voltage	427 V	660 V	673 V
Max Losses	5879 W	20912 W	6079 W

From this table the conclusion was made that **the 12 pole 72 slot out-runner was the one best suited for the task of generating electricity**. This due to its high power output at low rpms as well as low losses compared to the 10 pole 60 slot long configuration. The relatively high peak voltage was not deemed worse than controllable, furthermore it was concluded that the varying voltage from the machine was inevitable due to the varying rotational speed of the shaft.

Once the 12 pole 72 slot configuration was chosen a comparison of the weight to power ratio was done. In this comparison results from [22], a paper comparing cycloconverters and conventional generators was used. This comparison yielded the following results (figure 4.7) [22].

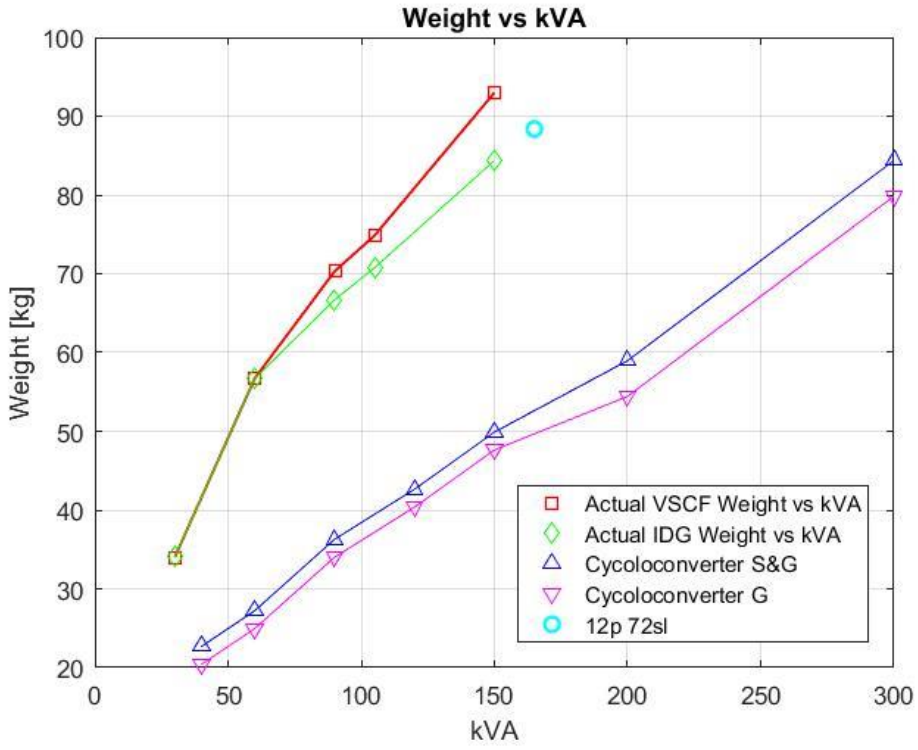

Figure 4.7.
Graph over weight to power ratio for different generator types. Abbreviation "*G*" stands for generator only and "*S&G*" stands for starter and generator.

From figure 4.7 it can be seen that the weight of the 12p 72sl is what can be expected of conventional generators of the same size. However the data used for figure 4.7 only looks at the weight of the generator itself and not the needed power electronics, therefore no final conclusion regarding total weight gain/loss can be taken at this point.

4.2 Maxwell 3D

The initial idea was to use Maxwell 3D in order to get a full 3D image of the loss distributions and other values. Unfortunately after spending over 30 hours with this software no model managed to run. Instead the data obtained from Maxwell 2D is deemed to be a good enough representation since most of the losses occurs in the core region of the generator. The main real loss not included by the 2D model is the strained losses in the windings on the side. It is however believed that cooling these should not be too much problem utilizing the proposed cooling mesh seen in figure 1.3 but further simulations are needed to prove this theory though.

Another thing that would be of interest to look in to for the generator is whether or not skewing of the stator could result in a more stable torque. As it is now the torque varies sharply up and down along the mean value. By skewing the stator this problem might be eliminated or at least improved in accordance with figure 4.8 below.

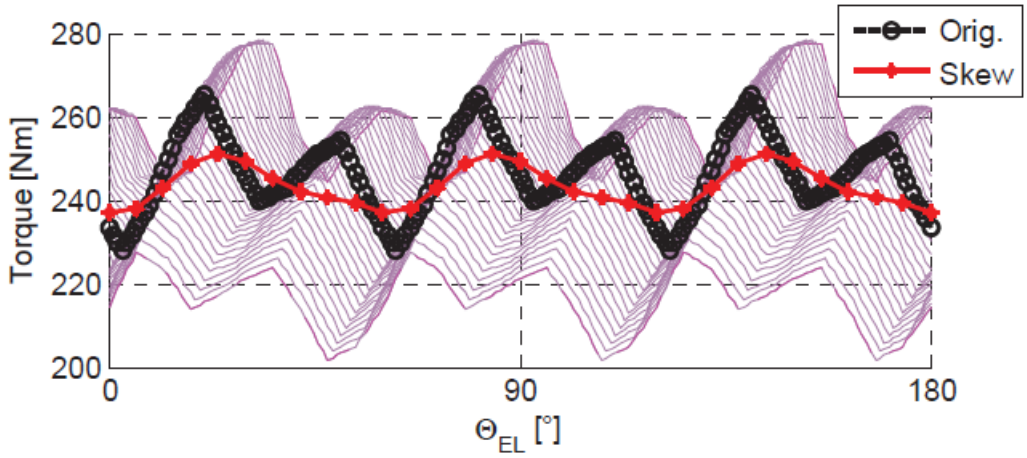

Figure 4.8.
Figure 4.8 displays the change in torque for a motor after applying skew to the stator, this example was taken from [23].

4.3 Mesh analysis

In order to establish the precision of the ANSYS Maxwell 2D analysis the 6744 rpm 400 amp of the “A, 10p 60sl (5) out-runner” simulation was run with an ever denser mesh grid. The mesh inputs for these simulations can be found in table 4.11 below and results from the simulations in the graph in figure 4.9.

Table 4.11.
Number of elements at different components during different simulations in ANSYS Maxwell 2D.

	Original	x2	x4	x8	x16	x32
Housing	540 ~	1080	2160	4320	8640	17280
Winding	120 ~	240	480	960	1920	3840
PM 1 & 2	900 ~	1800	3600	7200	14400	28800
Rotor	1330 ~	2660	5320	10640	21280	42560
Stator	1250 ~	2500	5000	10000	20000	40000

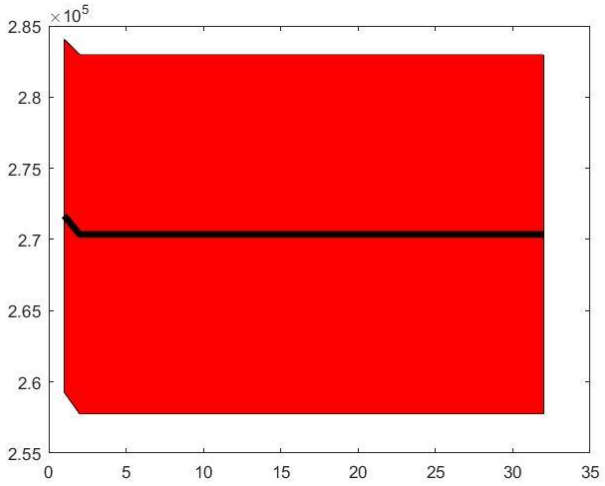

Figure 4.9.
Predicted power output for the suggested generator at ever denser mesh grid. The black line marks the rms value and the red area the std value.

As can be seen from figure 4.8 the mesh initial used can be seen as a good representation but for acquiring the best possible results the x2 settings are suggested.

4.4 GasTurb

Once the Generator has been analysed the engine itself is up next. It is found that the placement of the generator on the low pressure shaft instead of the high pressure shaft has a positive effect on the fuel economy, as well as overall performance. This subchapter provides a more in depth explanation of how this conclusion was reached.

In order to analyse the behaviour of the engine itself with the designed generator GasTurb 12 was used. This software offers a complete run through of the engine with the desired power off-take on the generator. There are in total nine different scenarios of interest for this simulation, these are operations at TOC, MTO and cruise conditions. Each of these conditions will be run with the following three configurations: generator connected to **HP** shaft, generator connected to **LP** shaft and **no generator**.

The simulations are run in three stages, first the TOC conditions are run for each of the three generator configurations, which gives the design layout of the engine. After that the MTO and cruise points are run in off-design in their respective generator based motor model.

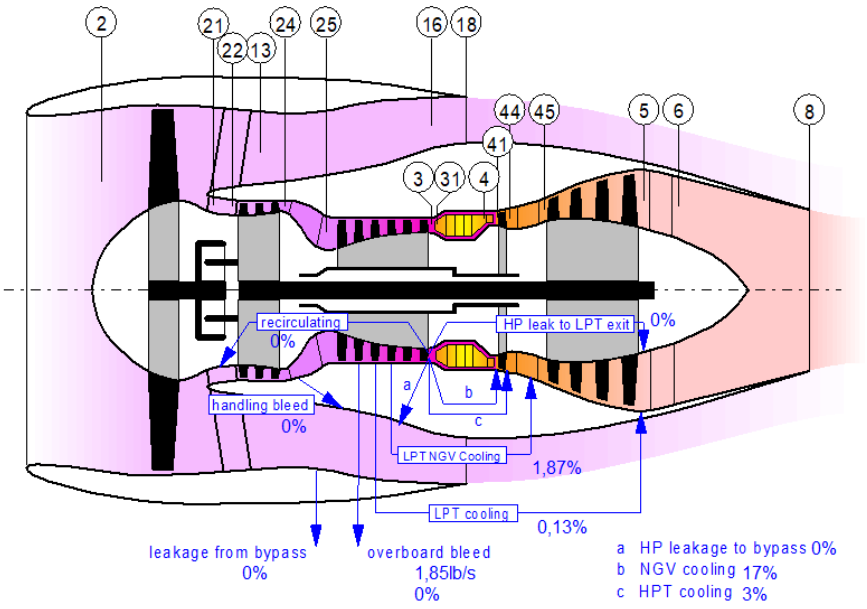

Figure 4.10.

Conceptual layout of the engine, as well as station (St) placement in accordance with GasTurb.

One of the most interesting results is how the specific fuel consumption varies dependent on flight conditions and generator configuration. The SFC can however be found directly in the GasTurb results and are as shown in table 4.12 below.

Table 4.12.
Specific fuel consumption for the engine at different operation points with different types of generator connection layout.

	TOC	MTO	Cruise
HP	100 %	100 %	100 %
LP	99.98 %	100 %	99.94%
No generator	99.45 %	99.66 %	99.22 %

As can be seen in table 4.12 the most efficient configuration is the no generator configuration. This comes as no surprise as the engine has a lower total load than the other and is only for reference to see what is lost when implementing the generator. However when looking at the results for the LP and HP configuration, it appears that the LP is more efficient than the HP in most aspects. The only point where the HP is preforming better than the LP is during MTO conditions but since most of the flight occurs with cruise conditions this is the flight conditions

that weighs the heaviest when looking at which configuration that is the most efficient. Based on data from [5] it can be assumed that the money saved as a function of SFC is 80000 USD per 0,1 % delta SFC. This gives a cost saving of 48000 USD during the aircrafts life span for cruise conditions.

Another thing that might be of interest to look at is the peak temperature in the engine. This can be found at station 4 and is as follows (see table 4.13 below).

Table 4.13.
Peak temperature (at station 4) for the engine at different operation points with different types of generator connection layout.

	TOC	**MTO**	**Cruise**
HP	1965.00 K	2011.75 K	1695.46 K
LP	1965.00 K	2011.41 K	1694.16 K
No generator	1965.00 K	2013.38 K	1692.98 K

From this it can be seen that no larger temperature difference exist and in fact the engine with no generator connected at all has the highest peak temperature which occur during MTO operation.

4.5 Other

This chapter will be dedicated to components which on their own might not take that much time and space to discuss but are equally important to the overall operations for the generator.

4.5.1 High power conductors from generator

Once the electrical power is generated within the EM it will be needed to be transported to the rest of the aircraft. The inside of the compressor housing does not however offer a very pleasant environment for cables to operate in. High and high currents among other things results in quite extreme operating conditions.

The maximum temperature inside the compressor housing during operations is 475 K with a RMS voltage of 388.3 volt and a peak current of 500 Amp. The cable chosen for these harsh conditions is the “FILOTEX BMS 13-58 T1 0000” this cable can operate in conditions varying between 208K (-65°C) and 533K (+260°C) and has a max RMS rating of 600 volts. The cable has a conducting diameter of 15.37 mm giving it a peak current density of around 3.77 A/mm^2 and a total diameter of 17.25 mm making it thin enough for installation within the engine [24].

4.5.2 Incoming oil tubing for cooling system

The tubing transporting oil to and from the cooling system with in the generator has a maximum volume flow of $0.0012\ m^3/s$ this is equal to 12 kW (6kW * 2 for safety). Assuming a maximum allowed flow speed of around 3.048 m/s ($10\ f/s$) based on [5]. If the oil is led through a tube with an inner diameter of 22.2 mm (14/16 inch) the cross section area is then $3.8795 \cdot 10^{-4}\ \ m^2$. This gives a flow speed of 3.0259 m/s resulting in a total of two tubes needed to transport the oil, one tube in and one tube out [5].

4.5.3 Structural support

To keep the stator in place, a number of spokes are connected between the cooling surface/manifold and the fan gearbox housing. In order to see how test the structural support of these a quick test was run. It was found that the current design of the spokes cannot live up to the limits that are set. This subchapter provides a more in depth explanation of how this conclusion was reached.

In order to see what kind of support the spokes would offer if implemented in the generator some quick calculations where preformed based on the equations listed below [5].

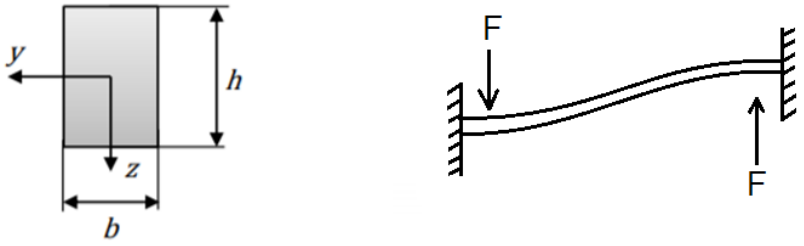

Figure 4.11.
Clarification of measurements and nomenclature.

$$\delta = \frac{F}{k} = \frac{F \cdot l^3}{6 \cdot E \cdot I} \qquad (4.1)$$

$$k = \frac{6 \cdot E \cdot I}{l^3} \begin{cases} I_y = \dfrac{bh^3}{12} \\ I_z = \dfrac{hb^3}{12} \end{cases} \qquad (4.2)$$

For an E-module value of 110 GPa (Titan 64), a b value of 8 mm, an h value of 25 mm as well as a length (l) of 230 mm the following results are obtained.

Table 4.14.
Calculated k values for the spokes connecting the stator to the gearbox.

Term	Value
$\boldsymbol{k_y}$	$5.65 \cdot 10^5\ [kg/s^2]$
$\boldsymbol{k_z}$	$5.79 \cdot 10^4\ [kg/s^2]$

The k value can then be used to calculate the angular frequency for the spokes with the following equation:

$$\omega = \sqrt{\frac{k}{m}} \qquad (4.3)$$

Here the mass is assumed to be 8.2 kg since there is ten spokes that are carrying the weight of the stator, this gives the following (see table 4.17).

Table 4.15.
Calculated angular frequency (ω) for the spokes connecting the stator to the gearbox.

Term	Value
$\boldsymbol{\omega_y}$	262.5 $[rad/s]$
$\boldsymbol{\omega_z}$	84.0 $[rad/s]$

In order to see if these values are god they can then be compared to the rotational speed of the HP shaft and for safeties sake a 20% safety margin is added.

Table 4.16.
Rpm values converted to rad/sec as well as with an added safety margin.

Condition	Rpm	Rad/sec	20 % safety
Cruise	3245	873.88	1048.7
MTO	9404	984.78	1181.7
TOC	9411	985.52	1182.6

As can be seen the spokes aren't even close to be able to withstand the forces within the engine. To get a better understanding of what would be needed to withstand these forces another test was run, this time with the following inputs: h = 40 mm and b = 40 mm. This results in a new mass of 1,79 kg per spoke compared of the original 0,22 kg. Running these values the following results are obtained.

Table 4.17.
Calculated k values for the spokes connecting the stator to the gearbox for the new sturdier spokes.

Term	Value
$\boldsymbol{k_y}$	$1.16 \cdot 10^7$ $[kg/s^2]$
$\boldsymbol{k_z}$	$1.16 \cdot 10^7$ $[kg/s^2]$

Table 4.18.
Calculated angular frequency (ω) for the spokes connecting the stator to the gearbox for the new sturdier spokes.

Term	Value
$\boldsymbol{\omega_y}$	1188.0 $[rad/s]$
$\boldsymbol{\omega_z}$	1188.0 $[rad/s]$

As can be seen this structure is sturdy enough to withstand the forces inside the engine but to the cost of dramatically increasing the mass of the spokes, the original spoke layout had a mas around 2,23 kg whilst the new have a mass of 17,85 kg. It is however believed that a smarter

design of the spokes could result in a sturdier structure but with a lower mass then the here presented 17,85 kg.

4.5.4 Weight of heat exchanger cooling unit

In order to get a better understanding of how the weight will change as a function of shifting to this type of system a preliminary weight comparison has been made below. Here all the weight that is lost as a function of removing the old system as well as weight gained by implementing the new can be found.

The weight of the heat exchanger is based on the heat exchanger located in the "RR AE3007 engine". This has an effect of 24,3 kW and a weight of 4,42kg it is assumed that it can be scaled linear which gives a mass of 2,18 kg for the 12 kW of effect needed in the RM400 [25]. The weight of the "Structural support for keeping the generator in place" is based on the assumption that this structure is constructed in titanium. Lastly the weight of the pump is assumed to be scalable to the CS-186 which has a volume flow of $2{,}52 \cdot 10^{-4}\ m^3/s$ and a weight off 0,66 kg, The flow for the system at hand is calculated to be $0{,}0012\ m^3/s$ which gives an approximated weight of 3,13 kg [26].

4.6 Implementation of system

The last thing that remains before concluding this paper is implementing everything discussed in this paper. It is concluded that the new power generation system will have an estimated weight of at least 105,55 kg but most likely more. This subchapter provides a more in depth explanation of how this conclusion was reached.

The only thing remaining in the end is the implementation of what has been done earlier in the paper. Based on the results from the simulations that has been run as well as the layout of the engine the following conceptual CAD model has been created to visualize the proposed generator layout (see figure 4.12). For a better understanding of the compressor in its entirety see figure 4.13.

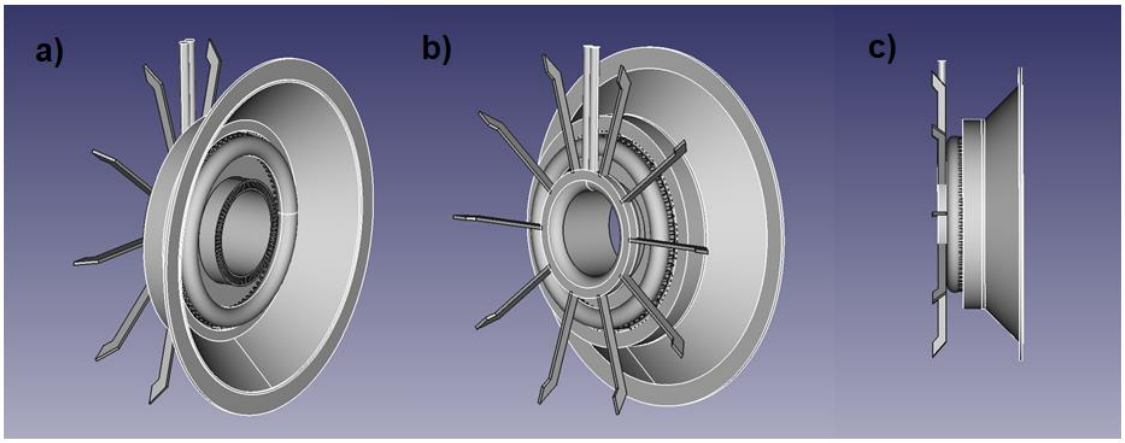

Figure 4.12.
Conceptual CAD model for the proposed LP generator.

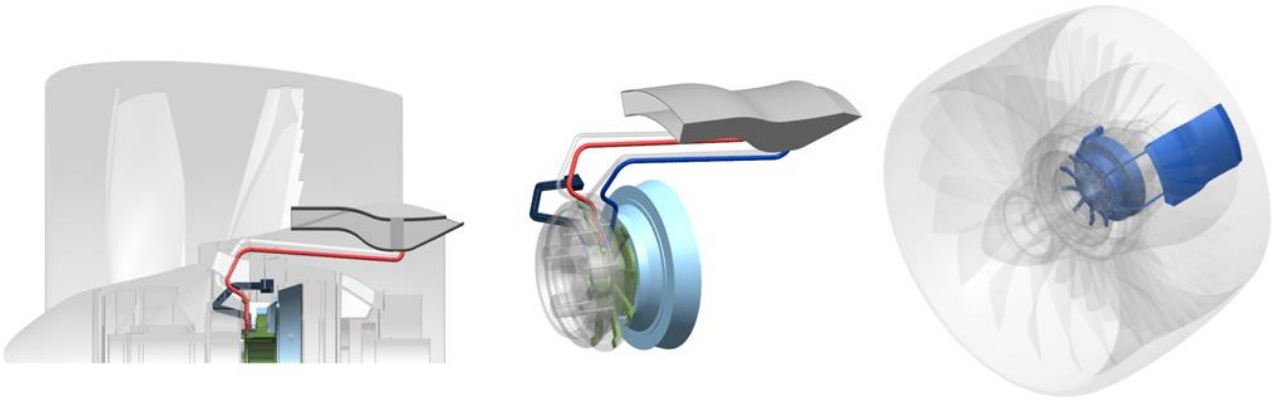

Figure 4.13.
Snapshot of the 12p 72sl generator implemented in the compressor.

The rotating part of the generator is to be connected to the compressor rotor, this is done through the cone to the right as seen in figure “4.12 c)”. The stator on the other hand will be connected to the fan gearbox this is done with the spokes (left side as seen in figure “4.12 c)”). The donut shape that can be seen in the most narrow part of figure “4.12 c)” and the inside of the cone in figure “4.12 a)” is a conceptual representation of the wiring sticking out of the generator on the sides. As for the two pipes on the stator side these are the cooling pipe which transports cooling oil to and from the generator. The cooling unit itself is the hollow mid structure that can be seen in figure “4.12 a)”.

Table 4.19.
Weight prediction of conventional system that can be lost and weight by proposed concept that will be gained if this system is implemented.

Conventional system		Proposed system (12p 72sl)	
CSD + Generator	76 kg	Generator	88,37 kg
Cable	3 kg	Cable	3,43 kg
Tubing for cooling	1,67 kg	Tubing for cooling	1,67 kg
Pump for cooling system	3,13 kg	Pump for cooling system	3,13 kg
Heat exchanger	2,18 kg	Heat exchanger	2,18 kg
Oil in the cooling system	1,5 kg	Oil in the cooling system	1,5 kg
Structural support for keeping the generator in place	10 kg	Structural support for keeping the generator in place	5,27 kg
Total weight	97,48 kg	Total weight	105,55 kg

The predictions for the 12p 72sl system made in table 4.19 are based in part on assumptions and approximation and can therefore vary a bit from the final product, for example the more robust

structure of the spokes is not used here, if it where the structural support should weigh 17.85 kg instead. It should also be mentioned that the weight prediction presented only looks at the weight in the engine and does not take the rest of the electronic system in to account. But from what can be seen the new generator configuration brings with it an increase of mass of about 8 kg per engine. Based on data from [5] the expected cost saving per kg is 1000 USD during the aircrafts life span, this results in a cost increase of 8070 USD as a result of the higher weight of the 12p 72sl compared to the conventional generator.

5 Conclusions and future work

5.1 Conclusion

From the MatLab simulations no real conclusion about the actual performance of the machine can be made. It is however believed to present a good base for looking at what a good layout would look like. The results from the RMxprt simulations are hard to validate, this is among other things due to the fact that they do not operate at low currents, which is a bit odd. The 2D models are however believed to give a more realistic representation of the actual output for the generator.

From the Electromagnetic design it is in the end believed that the generator can produce at least the amount of power desired by GKN. Of the two models capable of producing this power the 12 pole 72 slot generator configuration is believed to be the best one.

From the mesh analysis it is concluded that the results obtained from the simulations are a good representation of reality according to ANSYS Maxwell. Unfortunately no 3D analysis of the problem could be run due to problems with the software.

After running the GasTurb simulations it was concluded that placing the generator on the LP shaft instead of the HP shaft will result in an improved SFC of 0,06 % during cruise conditions.

When it comes to fitting the generator within the motor no bigger problems can be found and from what can be seen no initial problem seems to exist with the wiring and cooling connected to the generator. The new proposed 12p 72sl generator is expected to add somewhere around 8 kg of mass to each engine. This paper does not however take the rest of the airplane in to account.

The total cost saving during the aircrafts lifetime as a result of the improved SFC combined with the increased weight of the engine is calculated to be approximately 39930 USD. Whilst the improved SFC gives a decrease in cost of 48000 USD the increase of weight results in an increase of cost equal to 8070 USD. It should however be mentioned that the weight of the new generator unit is at this point approximated and might increase in a later stage.

When it comes to dimensioning the generator the lowest rpm conditions sets the bar for the generator. In order to be able to generate enough electrical power the generator needs to be big enough. At higher rpms however this generator far out performs what is needed of it. In table 5.1 below outputs for the generator at different conditions are displayed assuming a current of 500 Amp.

Table 5.1.
Power excess for operations with current of 500 Amp.

	Ground idle	**Cruise**	**MTO**	**TOC**
Power need, kW	123	123	156,6	123
Power delivered, kW	123	514	558	574
Power delivered, %	100 %	418 %	356 %	467 %

As can be seen the power that can actually be produced at for example cruise conditions are 418 % of what is needed. It is believed that this should be enough to replace the current ac-system that requires bleed air to operate with dedicated compressors as seen on the 787. This would in turn further improve the fuel economy since less energy would be lost in bleed.

Further work is still needed on numerous areas which can be found listed under chapter *5.2 Future work*.

5.2 Future work

As mentioned earlier this study is just an initial look at implementing an integrated generator for compressors and several other things will have to be investigated further before implementing this concept in reality.

5.2.1 Optimization of design

One major thing that needs to be investigated before further development of the proposed generator is optimization. In this paper some basic optimization has been done but not enough to guarantee there is no better layout exists that takes the same amount of space or less.

It might also be of interest to test another type of rotor with varying magnetization. This would most likely offer a better control of torque generation as well as a more even level off voltage during operation.

5.2.2 Solidity

The solidity of the generator needs to be tested as well, in this paper no bigger interest has been put at looking into if the generator can withstand the immense forces it is exposed to during operations. What changes to the structural support will be needed can be seen in chapter “4.7 Implementation of system”. However the exact nature of these changes are hard to predict, this is among other things due to the fact that the layout presented in this paper might not be what will be used in the end (see chapter “5.2.1 Optimization of design”). Therefore further simulations are needed before any exact values can be listed. During these tests vibrations in the structure needs to be evaluated as well.

5.2.3 Heat transfer

Initially one of the goals for this paper was to look into the heat transfer process of the EM. This was in order to see if the generated heat could be cooled with the integrated cooling in the housing without overheating the copper winding. Unfortunately no heat transfer analysis was preformed due to problems with the software and therefore needs to be run before implementation of this concept.

5.2.4 Cooling in wires

Another thing of interest is further development of the cooling, an integrated cooling system in the wiring of the generator could offer a better cooling as well as the possibility of running on higher amp values and better utilize the generator.

5.2.5 3D analysis

It is unfortunate that the 3D tool in Maxwell would not work as whished during this project. Another test that therefore would be of interest is to run 3D electromagnetic simulations of the generator in order to see if these results would wary from what can be seen in the 2D case.

5.2.6 Electronics

In this paper no bigger effort has been placed on the electronics outside the generator itself. However before this concept can be implemented a more detailed look needs to be taken at this area. This since some type of power electronics will be needed to regulate the voltage of the generators since this value varies depending on rotational speed of the shaft.

In the current market the Boeing 787 utilizes numerous different voltage ratings and sifting between AC and DC [4]. With this in mind it is in this paper assumed that cables can be drawn directly from the generator all the way to the "aft electronics equipment bay" where the power supplied by the generator will be converted before being distributed all over the aircraft. In a paper published by Hartmann rectifiers similar to what can be found aboard a 787 calculated a power density of about 14,1 kW per dm^3 which may serve as a first approximation of size for the system [27]. Further studies are however as mentioned needed before implementing this type of system.

5.2.7 Maintenance

As the concept reaches a more defined layout and technical specifications a closer look will be needed on the maintenance aspects of the engine. This in order to see how the need for maintenance for the new concept varies from the old as well as the time requirements for this maintenance.

5.2.8 Safety

This new design also brings some new challenges when it comes to safety. Since the rotor is connected directly to the LP-shaft it won't be possible to stop the generator from rotating during flight without turning of the motor.

5.2.9 Economics and logistics

Another important factor that needs to be investigated further are the economics of the generator. Can it be produced cheaper than the rivalling systems? What are the installation costs? What is the life expectancy for one of these units? How much will the research and development cost for this project be? All these questions and more will be needed to be investigated further if this project is to be used on the market. If the project however mostly serves to answer a curiosity these questions can wait till the end of the research and development phase. In order to implement this new type of generator in to existing engines the following is needed: research and development, manufacturing setup and manufacturing logistics. This whilst the IDG only needs to be manufactured since the other things already have been done.

A closer look at the exact change in fuel consumption is also needed. In this paper no effort has been placed in this area due to the highly iterative nature of this problem.

References

[1] T. Bäckström, 2001, *NFFP 'All Electrical Vehicle'*, Stockholm, Kungliga Tekniska Högskolan

[2] R. Abdel-Fadil, A. Eid, M. Abdel-Salam, 2013, *Electrical Distribution Power Systems of Modern Civil Aircrafts*, Cairo

[3] J. Karimi, 2007, *Future Aircraft Power Systems- Integration Challenges*

[4] M. Sinnett, 2007, *787 No-Bleed Systems: Saving Fuel and Enhancing Operational Efficiencies*, Aero Magazine

[5] Internal GKN data

[6] J. Chang, C. H. LeMond, A. Wang, 2004, *Distributed system and methodology of electrical power regulation, conditioning and distribution on an aircraft US 6778414 B2*, 2004-08-17, https://www.google.com/patents/US6778414

[7] E. Richter, D. H. Anstead, J. W. Bartos, T. U. Watson, 1995, *Preliminary Design of an Internal Stater/ Generator for Application in the F110-129 Engine*, Warrendale, SAE

[8] I. Moir, A. Seabridge, 2013, *Design and Development of Aircraft Systems*, Second Edition, West Sussex, John Wiley & Sons

[9] E. Ganev, 2015, *Electric Machines for Electrical Power Generation Systems*, IEEE Electrification Magazine

[10] Dura Magnetics Inc, 2017, *Temperature Effects on Samarium Cobalt Magnets*, 2017-10-17, https://www.duramag.com/samarium-cobalt-magnets-smco/temperature-effects-on-samarium-cobalt-magnets/

[11] W. Tong, 2014, *Mechanical Design of Electric Motors*, Boca Raton, CRC Press

[12] T. J. E. Miller, 1989, *Brushless Permanent-Magnet and Reluctance Motor Drives*, Oxford, Clarendon Press

[13] Cogent Surhammars Bruk AB, 2008, *M235-50A*

[14] Marathon Generators, 2015, *Insulation System Thermal Life Expectancy vs Total Operating Temperature*

[15] Y. Zhang, M. Cheng, P. Pillay 2009, *Magnetic Characteristics and Excess Eddy Current Losses*, IEEE

[16] Bengt Sundén, 2012, *Introduction to Heat Transfer*, WITPress Southampton, Boston, 1st edition

[17] viscopedia, 2017, *Engine Oil*, 2017-11-20, http://www.viscopedia.com/viscosity-tables/substances/engine-oil/

[18] W. Scott, S. Paul, P, Harold, S. Ernest E. 2005, *HEAT TRANSFER PROPERTIES OF ENGINE OILS*, Washington, D.C.

[19] K. Stephan, A. Laesecke, 1985, The Thermal Conductivity Of Fluid Air, J. Phys. Chem. Ref. Data,Vol 14, No 1

[20] K. Stephan, A. Laesecke, https://www.ohio.edu/mechanical/thermo/property_tables/air/air_Cp_Cv.html J. Phys. Chem. Ref. Data, Vol 14, No 1, 1985.

[21] Anderson, Jr., J. D, 2011, *Fundamentals of Aerodynamics*, 5th Edition, McGraw-Hill

[22] General Electric Company, 1980, *Samarium Cobalt (SmCo) Generator/Engine Integration Study*, Ohio

[23] R. Andersson, A Reinap, M Alaüla, 2016, *'Engineering considerations on skewing of an interior permanent magnet synchronous machine for parallel hybrid electric heavy vehicles'*, Lund, Lund University

[24] Nexans, *Aircraft Wires and Cables*, 2018-02-01, http://www.nexans.com/Poland/2007/Aircraft.pdf

[25] AMETEK, 2005, *Surface Air/Oil Cooler*, 2018-01-22 http://www.nasco.co.jp/cms/mark/pdf/AMETEK_HT/Surface_Aire-Oil_Cooler.pdf

[26] Cascon, *Oil Scavenge Pump for Aircraft Electric Generator*, 2018-01-22, https://www.casconpump.com/product/oil-scavenge-pump-for-aircraft-electric-generator/

[27] M. Hartmann, 2011, *Ultra-Compact and Ultra-Efficient Three-Phase PWM Rectifier Systems for More Electric Aircraft*, ETH Zurich